Geophysical Prospecting EAGE EUROPEAN ASSOCIATION OF GEOSCIENTISTS & ENGINEERS

Geophysical Prospecting doi: 10.1111/1365-2478.12011

Seismic characterization of naturally fractured reservoirs using amplitude versus offset and azimuth analysis

Mehdi E. Far[1*], Colin M. Sayers[1,2], Leon Thomsen[1,3], De-hua Han[1] and John P. Castagna[1]

[1] *University of Houston*
[2] *Schlumberger and* [3] *Delta Geophysics*

Received March 2012, revision accepted September 2012

ABSTRACT

P-wave seismic reflection data, with variable offset and azimuth, acquired over a fractured reservoir can theoretically be inverted for the effective compliance of the fractures. The total effective compliance of a fractured rock, which is described using second- and fourth-rank fracture tensors, can be represented as background compliance plus additional compliance due to fractures. Assuming monoclinic or orthotropic symmetry (which take into account layering and multiple fracture sets), the components of the effective second- and fourth-rank fracture compliance tensors can be used as attributes related to the characteristics of the fractured medium. Synthetic tests indicate that using *a priori* knowledge of the properties of the unfractured medium, the inversion can be effective on noisy data, with S/N on the order of 2. Monte Carlo simulation was used to test the effect of uncertainties in the *a priori* information about elastic properties of unfractured rock. Two cases were considered with Wide Azimuth (WAZ) and Narrow Azimuth (NAZ) reflection data and assuming that the fractures have rotationally invariant shear compliance. The relative errors in determination of the components of the fourth-rank tensor are substantially larger compared to the second-rank tensor, under the same assumptions.

Elastic properties of background media, consisting in horizontal layers without fractures, do not cause azimuthal changes in the reflection coefficient variation with offset. Thus, due to the different nature of these properties compared to fracture tensor components (which cause azimuthal anomalies), simultaneous inversion for background isotropic properties and fracture tensor components requires additional constraints.

Singular value decomposition (SVD) and resolution matrix analysis can be used to predict fracture inversion efficacy before acquiring data. Therefore, they can be used to determine the optimal seismic survey design for inversion of fracture parameters. However, results of synthetic inversion in some cases are not consistent with resolution matrix results and resolution matrix results are reliable only after one can see a consistent and robust behaviour in inversion of synthetics with different noise levels.

Key words: Fractures, AVOA, Reflection coefficient, Inversion, Singular value decomposition.

* Email: mehdi.eftekhari@luminageo.com

INTRODUCTION

Natural and induced fractures in reservoirs play an important role in determining fluid flow during production and knowledge of the orientation and density of fractures is useful to optimize production from fractured reservoirs (e.g., Reiss 1980; Nelson 1985). Areas of high-fracture density may represent zones of high permeability, therefore locating wells in these areas may be important. Fractures usually show preferred orientations and this may result in significant permeability anisotropy in the reservoir. It is important for optimum drainage that producers should be more closely spaced along the direction of minimum permeability than along the direction of maximum permeability and the azimuthal orientation of deviated wells should be chosen to maximize production taking into account the orientation of fractures (Sayers 2009).

Seismic anisotropy is defined as the dependence of seismic velocity upon angle. Seismic velocity anisotropy can be caused by different factors, such as rock fabric, grain-scale microcracks, rock layering and aligned fractures at all scales, provided that the characteristic dimensions of these features are small relative to the seismic wavelength (Worthington 2008). As a result, P-waves propagating parallel to fractures will be faster than those propagating perpendicular to fractures (Fig. 1).

The use of seismic waves to determine the orientation of fractures has received much attention. For example, Lynn *et al*. (1994) used the azimuthal variation in the reflection amplitude of seismic P-waves to characterize fractured reservoirs (see also Eftekharifar and Sayers 2011a, b). Reflection amplitudes have advantages over seismic velocities for characterizing fractured reservoirs because they have higher vertical resolution. However, the interpretation of variations in reflection amplitude requires a model of sufficient complexity to allow the measured change in reflection amplitude to be inverted correctly for the characteristics of the fractured reservoir (Sayers 2009).

Current models used to invert the seismic response of fractured reservoirs often make simplified assumptions that prevent fractured reservoirs from being characterized correctly. Many models assume a single set of perfectly aligned fractures (e.g., Mallick, Chambers and Gonzalez 1996; Sayers and Rickett 1997; Rüger 1997). But consider a vertically fractured reservoir containing a large number of fractures of the same type with normals that are isotropically distributed in the horizontal plane. For this example, there will be little or no variation in the reflection coefficient with azimuth and an interpretation of the reflection amplitude-versus-azimuth curve using an assumption of a single set of aligned fractures would predict incorrectly that the fracture density is zero (Sayers 2009). Hence it is important to consider the possibility that reservoirs contain several sets of fractures with variable orientation within a given fracture set, as illustrated in Fig. 2 (see, for example, Sayers 1998; Sayers and Dean 2001; Far 2011).

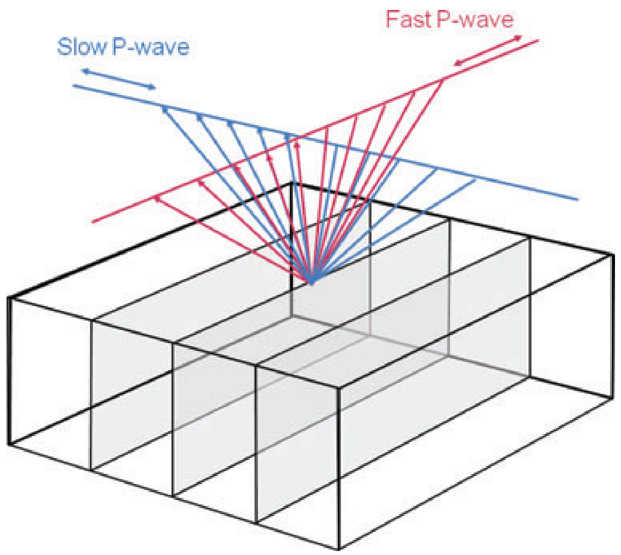

Figure 1 Reflection from a fractured layer with a single set of parallel vertical fractures for acquisition parallel and perpendicular to the fractures

Figure 2 Orthotropic (top) and monoclinic (bottom) symmetries in fractured sandstone, Arches National Monument.

The simple model of Horizontally Transverse Isotropic (HTI) symmetry, which assumes one set of aligned vertical fractures (with rotationally invariant shear compliance) embedded in an otherwise isotropic background is misleading for another reason. In the HTI model, horizontal layering of sediments, leading to a variation of velocity with polar angle, is ignored. Hence HTI is not a suitable model in sedimentary basins, where layering is ubiquitous and no fractures can be presumed to lie within an 'otherwise isotropic background', although it may be useful in the igneous crust, for which it was originally proposed (e.g., Crampin 1984).

In this work, the linear slip theory (see below) is used to describe the relation between stress and fracture strain, as expressed by the specific compliances of the fractures. This theory describes fractures using normal and tangential specific compliances of fractures, without detailed assumptions concerning the microgeometry of the fractures. It is assumed that the specific shear compliance of fractures is rotationally invariant around the normal to the fractures (this work will be generalized in a future paper to the case of rotationally-dependent shear compliance, enabling the analysis of joints, which are much longer horizontally than vertically.) Thomsen (1995) showed the effect of frequency and squirt flow on elastic properties of fractured rocks, including their interaction with equant (non-fracture) porosity. At higher frequencies, fluid-filled fractures tend to be stiffer than at lower frequencies. Based on data from several authors, Worthington (2008) showed that fracture specific compliances are directly related to fracture dimension. The theory developed by Kachanov (1980) and Sayers and Kachanov (1991, 1995) is used for effective medium modelling of media with fractures having rotationally invariant shear compliance. Kachanov (1980) applied this approach to modelling permeability also.

Fracture characterization using surface seismic data demands wide azimuth surveys. Due to the high cost of wide azimuth seismic data acquisition, the determination of azimuth/offset characteristics in such data, for the task of fracture modelling, becomes very important, as does optimization of the acquisition for revealing such characteristics. This optimization will be demonstrated using Singular Value Decomposition (SVD) and inversion of synthetic Amplitude Versus Offset and Azimuth (AVOA) data. Synthetic AVOA data for differently oriented vertical fractures are analysed, in order to identify which parameter combinations are well-resolved by various experimental geometries. Synthetic reflectivity data are also used to invert for the components of the additional effective fracture compliance tensor. Inversion results are in general consistent with resolution matrix results with different noise levels, proving the usefulness of SVD for this inverse problem.

LINEAR SLIP CONDITION

The small vector difference (across a fracture) in the displacement field $\boldsymbol{u}$ is assumed to depend linearly on the traction vector $\boldsymbol{t}$. This dependence may be assumed to be real and frequency independent, corresponding to an elastic spring condition, or it may be assumed to be complex and frequency dependent (Jones and Whittier 1967; Schoenberg 1980).

For a smoothly curved surface between two elastic media, assume a coordinate system with x_1 and x_3 in directions tangential to the local fracture plane and x_2 perpendicular to that fracture plane. We will assume here that the fractures are vertical, with orientations in the horizontal plane to be determined by analysis. Let $\boldsymbol{u}$ denote displacement (see Fig. 3) and

$$\Delta \boldsymbol{u} = \boldsymbol{u}^R - \boldsymbol{u}^L, \tag{1}$$

be the difference, or discontinuity of displacement, between the right (R) fracture face and left (L) fracture face. The time dependency is suppressed. The traction vector $\boldsymbol{t}$ we take as the second row of the stress tensor, with components σ_{21}, σ_{22} and σ_{23}, which are the forces per unit area that the material on the $+x_2$ side of the interface exerts on the $-x_2$ side. It is assumed, following Schoenberg (1980), that the traction is

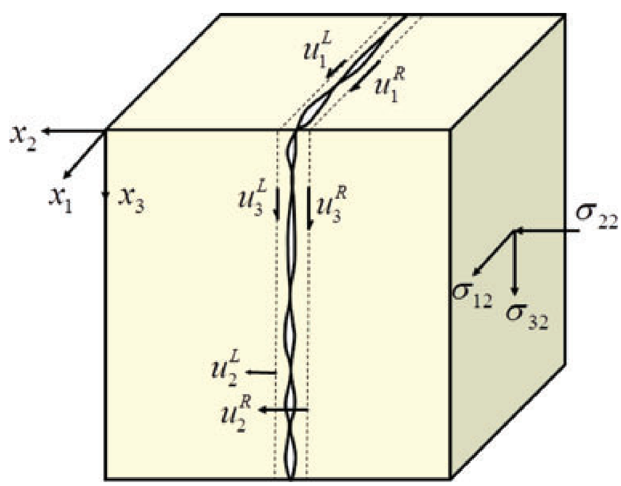

Figure 3 The normal and tangential displacements at the face of the fracture are denoted by u_3, u_1 and u_2. The normal and tangential components of the displacement discontinuity at the fracture are given by $\Delta u_i = u_i^R - u_i^L$ and are related to the normal and shear tractions.

linearly dependent on the displacement slip:

$$\boldsymbol{t}(\Delta\boldsymbol{u}) \approx \boldsymbol{k}\Delta\boldsymbol{u}, \tag{2}$$

where $\boldsymbol{k}$ is the specific stiffness matrix.

If the specific stiffness matrix $\boldsymbol{k}$ is required to be invariant with respect to inversion of x_2, it can be shown (Schoenberg 1980) that off-diagonal terms k_{21}, k_{12}, k_{32} and k_{23}, between the normal and tangential directions, must be zero. If there is rotational symmetry for shear compliance around the x_2 axis, it can be shown that $k_{13} = k_{31} = 0$, $k_{11} = k_{33} = k_T$ and $k_{22} = k_N$ (Schoenberg 1980).

It is convenient to characterize compliances instead of stiffnesses, which are the inverse of a compliance matrix. One can write (Kachanov 1980):

$$\Delta\mathbf{u} = \begin{bmatrix} B_T & 0 & 0 \\ 0 & B_N & 0 \\ 0 & 0 & B_T \end{bmatrix}\mathbf{t}, \tag{3}$$

where $B_N = {k_N}^{-1}$ and $B_T = {k_T}^{-1}$ are the normal and tangential specific fracture compliances respectively and their dimension is length/stress. B_N gives the displacement discontinuity in the direction normal to the fracture for a unit normal traction and B_T gives the displacement discontinuity parallel to the fracture plane for unit shear traction (see Fig. 3). If there are multiple fractures, then the effective compliances of a given fracture will be affected by the presence of the other fractures. They also depend on the fluid content and fracture density. In index notation, equation (3) is:

$$\Delta u_i = B_{ij} t_j, \tag{4}$$

with $B_{11} = B_{33} = B_{\mathrm{T}}$ and $B_{22} = B_{\mathrm{N}}$. The specific compliance tensor $\boldsymbol{B}$ above is written for the case of fractures with rotationally invariant shear compliance, normal to the x_2 direction; for a fracture with arbitrary orientation, it may be written compactly as (Kachanov 1980):

$$B_{ij} = B_{\mathrm{N}} n_i n_j + B_T(\delta_{ij} - n_i n_j). \tag{5}$$

The boundary conditions shown in equation (4) were first used by Jones and Whittier (1967) for modelling of wave propagation through a flexibly bonded interface by allowing both slip and separation. The vanishing of either or both of these specific compliances leads to perfectly bonded interface conditions. Real elastic parameters may be generalized to complex frequency- dependent viscoelastic parameters, therefore linear viscoelastic interfaces can be modelled as well (Schoenberg 1980).

Schoenberg's linear slip theory was originally developed for a single set of fractures (with rotationally invariant shear compliance) embedded in isotropic host rock and later was extended to several fracture sets (see, for example, Schoenberg and Muir 1989; Schoenberg and Sayers, 1995) and also to anisotropic backgrounds (e.g., Sayers and Kachanov 1991, 1995; Helbig 1994; Schoenberg and Sayers 1995).

ARBITRARY VERTICAL FRACTURES

In an elastic medium that contains an arbitrary number of sets of fractures with arbitrary orientation distribution, using the divergence theorem and Hooke's law, it can be shown (Hill 1963; Sayers and Kachanov 1995) that the elastic compliance tensor of the fractured medium can be written in the following form:

$$S_{ijkl} = S^0_{ijkl} + \Delta S_{ijkl}, \tag{6}$$

where $\boldsymbol{S}^0$ is the compliance matrix of the medium (including the effects of pores, cracks and stress except for those fractures explicitly included in $\Delta\boldsymbol{S}$).

Following Nichols, Muir and Schoenberg (1989), the additional (effective) compliance matrix $\Delta\boldsymbol{S}$, for n sets of aligned fractures can be written as:

$$\Delta\boldsymbol{S} = \sum_{q=1}^{n} \Delta\boldsymbol{S}^q, \tag{7}$$

where $\Delta\boldsymbol{S}^q$ is the additional effective compliance matrix of the q^{th} set of aligned fractures in the presence of the other fracture sets. Implicitly, each of these effective fracture compliances depends upon the rest of the rock, specifically including the presence, location, size and orientation of the other fractures and pores (including their intersections, if liquid-filled).

Sayers and Kachanov (1991, 1995) derived the effective additional compliance matrix due to fractures with rotationally invariant shear compliance. Using equations (6)–(8), the effective excess compliance ΔS_{ijkl} due to the presence of the fractures can be written as:

$$\Delta S_{ijkl} = \frac{1}{4}(\delta_{ik}\alpha_{jl} + \delta_{il}\alpha_{jk} + \delta_{jk}\alpha_{il} + \delta_{jl}\alpha_{ik}) + \beta_{ijkl}. \tag{8}$$

Here, δ_{ij} is the Krönecker delta, α_{ij} is a second-rank tensor and β_{ijkl} is a fourth-rank tensor defined by:

$$\alpha_{ij} = \frac{1}{V}\sum_r B_T^{(r)} n_i^{(r)} n_j^{(r)} A^{(r)}, \tag{9}$$

$$\beta_{ijkl} = \frac{1}{V}\sum_r \left(B_{\mathrm{N}}^{(r)} - B_T^{(r)}\right) n_i^{(r)} n_j^{(r)} n_k^{(r)} n_l^{(r)} A^{(r)}, \tag{10}$$

where the sum is over all fractures in volume V. Variable ${n_i}^{(r)}$ is the i^{th} component of the normal to the r^{th} fracture and $A^{(r)}$

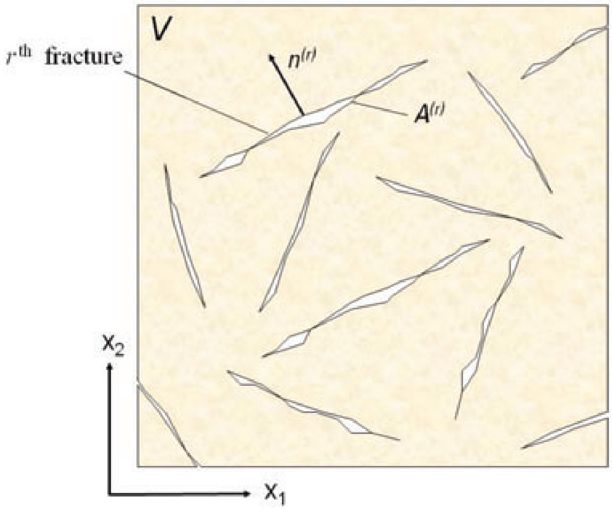

Figure 4 Horizontal section through volume V containing N vertical fractures, where the r^{th} fracture has area $A^{(r)}$ and normal $n^{(r)}$.

is the area of the r^{th} fracture (see Fig. 4). Note that α_{ij} and β_{ijkl} are both invariant to all permutations of the indices.

For the case of gas-filled or 'dry' fractures, since normal and shear compliance of the fractures are almost equal (see Sayers and Kachanov 1995), the effect of the fourth-rank tensor β can be neglected (see equation (10)) in this case. If the fractures are filled with liquid and if the volume V contains equant porosity in addition to fracture porosity, there may be fluid flow between fractures and equant pores (Thomsen 1995). This effect helps to determine the values of the specific fracture compliance, particularly B_N.

Since specific compliances (B_{ij}) depend on the fracture interaction, fluid content, etc., the excess compliance matrix ΔS (e.g., α and/or β) will also depend on these factors. Thus, an effective fracture compliance can be defined that implicitly takes into account all the interactions between fractures. We can invert this effective fracture compliance from azimuthally varying surface PP- seismic data (see inversion results, below). However it should be noted that interpretations of the inversion results for implicit effective compliances cannot be unique and one can only draw conclusions about relative effects of the fractures (as opposed to absolute effects).

The discussion above does not mean that the effect of fractures is 'additive', because in summing fracture compliances, all the compliances of individual fractures depend implicitly on the existence of the other fractures, so if we double the number of fractures, the total fracture compliance does not double, since now all of the original fractures have different effective compliances and the new fractures similarly interact with the originals.

Some numerical studies have reported that fracture interactions do not have a significant effect on the total elastic behaviour of dry fractured media (e.g., Grechka and Kachanov 2006). These studies had the following assumptions:

(1) They assumed zero fracture volume
(2) The concentrations and crack densities were dilute
(3) They ignored microfractures and porosity in the host rock between macrofractures
(4) They ignored fluid effects
(5) They considered very specific geometries.

In the formulation presented here, fracture compliances are taken to be 'effective' (in the presence of other fractures) and thus the assumption of non-interaction is not required.

If there is only a single set of perfectly aligned vertical fractures, equations (9) and (10) become

$$\alpha = N_V \bar{A}\bar{B}_T \begin{bmatrix} \sin^2\varphi & \cos\varphi\sin\varphi & 0 \\ \cos\varphi\sin\varphi & \cos^2\varphi & 0 \\ 0 & 0 & 0 \end{bmatrix}, \tag{11}$$

$$\beta = N_V \bar{A}(\bar{B}_N - \bar{B}_T) \begin{bmatrix} \sin^4\varphi & \sin^2\varphi\cos^2\varphi & 0 & 0 & 0 & 2\sin^3\varphi\cos\varphi \\ \sin^2\varphi\cos^2\varphi & \cos^4\varphi & 0 & 0 & 0 & 2\sin\varphi\cos^3\varphi \\ 0 & 0 & 0 & 0 & 0 & 0 \\ 0 & 0 & 0 & 0 & 0 & 0 \\ 0 & 0 & 0 & 0 & 0 & 0 \\ 2\sin^3\varphi\cos\varphi & 2\sin\varphi\cos^3\varphi & 0 & 0 & 0 & 4\sin^2\varphi\cos^2\varphi \end{bmatrix}, \tag{12}$$

where N_V is the number of fractures per unit volume, $\bar{A}$ is the average area of the fractures in the set, $\bar{B}_T$ and $\bar{B}_N$ are the (area-weighted) average specific tangential and normal compliances and φ is the azimuthal angle between the fracture strike and the survey 1-axis. The factors of 2 and 4 in column 6 arise from the fact that for compliances (including these additional compliances), as opposed to stiffnesses,

$$\beta_{16} = 2\beta_{1112}, \quad \beta_{26} = 2\beta_{2212}, \quad \beta_{66} = 4\beta_{1212}, \tag{13}$$

according to the Voigt two-index notation. It is shown in the Appendix A that, if the background medium is isotropic, this case yields 'HTI' symmetry, which as discussed above is not a suitable approximation in sedimentary basins. If the background medium is polar anisotropic, this case yields orthotropic symmetry.

If there are two sets of perfectly aligned vertical fractures, oriented orthogonally, then equations (9) and (10) become:

$$\alpha = N_{V1}\bar{A}_1\bar{B}_{T1}\begin{bmatrix} \sin^2\varphi_1 & \cos\varphi_1\sin\varphi_1 & 0 \\ \cos\varphi_1\sin\varphi_1 & \cos^2\varphi_1 & 0 \\ 0 & 0 & 0 \end{bmatrix} + N_{V2}\bar{A}_2\bar{B}_{T2}\begin{bmatrix} \cos^2\varphi_1 & -\sin\varphi_1\cos\varphi_1 & 0 \\ -\sin\varphi_1\cos\varphi_1 & \sin^2\varphi_1 & 0 \\ 0 & 0 & 0 \end{bmatrix}, \tag{14}$$

$$\beta = N_{V1}\bar{A}_1(\bar{B}_{N1}-\bar{B}_{T1}) \times \begin{bmatrix} \sin^4\varphi_1 & \sin^2\varphi_1\cos^2\varphi_1 & 0 & 0 & 0 & 2\sin^3\varphi_1\cos\varphi_1 \\ \sin^2\varphi_1\cos^2\varphi_1 & \cos^4\varphi_1 & 0 & 0 & 0 & 2\sin\varphi_1\cos^3\varphi_1 \\ 0 & 0 & 0 & 0 & 0 & 0 \\ 0 & 0 & 0 & 0 & 0 & 0 \\ 0 & 0 & 0 & 0 & 0 & 0 \\ 2\sin^3\varphi_1\cos\varphi_1 & 2\sin\varphi_1\cos^3\varphi_1 & 0 & 0 & 0 & 4\sin^2\varphi_1\cos^2\varphi_1 \end{bmatrix} + N_{V2}\bar{A}_2(\bar{B}_{N2}-\bar{B}_{T2}) \times \begin{bmatrix} \cos^4\varphi_1 & \cos^2\varphi_1\sin^2\varphi_1 & 0 & 0 & 0 & -2\cos^3\varphi_1\sin\varphi_1 \\ \cos^2\varphi_1\sin^2\varphi_1 & \sin^4\varphi_1 & 0 & 0 & 0 & -2\cos\varphi_1\sin^3\varphi_1 \\ 0 & 0 & 0 & 0 & 0 & 0 \\ 0 & 0 & 0 & 0 & 0 & 0 \\ 0 & 0 & 0 & 0 & 0 & 0 \\ -2\cos^3\varphi_1\sin\varphi_1 & -2\cos\varphi_1\sin^3\varphi_1 & 0 & 0 & 0 & 4\cos^2\varphi_1\sin^2\varphi_1 \end{bmatrix}, \tag{15}$$

where φ_1 is the azimuthal angle between the fracture set with label 1 and the survey 1-axis. It is shown in Appendix A that this results in orthotropic symmetry.

If the two fracture sets are not orthogonal but are perfectly aligned (within each set), then equations (14) and (15) become,

$$\alpha = N_{V1}\bar{A}_1\bar{B}_{T1}\begin{bmatrix} \sin^2\varphi_1 & \cos\varphi_1\sin\varphi_1 & 0 \\ \cos\varphi_1\sin\varphi_1 & \cos^2\varphi_1 & 0 \\ 0 & 0 & 0 \end{bmatrix} + N_{V2}\bar{A}_2\bar{B}_{T2}\begin{bmatrix} \sin^2\varphi_2 & \cos\varphi_2\sin\varphi_2 & 0 \\ \cos\varphi_2\sin\varphi_2 & \cos^2\varphi_2 & 0 \\ 0 & 0 & 0 \end{bmatrix}, \tag{16}$$

$$\beta = N_{V1}\bar{A}_1(\bar{B}_{N1}-\bar{B}_{T1}) \times \begin{bmatrix} \sin^4\varphi_1 & \sin^2\varphi_1\cos^2\varphi_1 & 0 & 0 & 0 & 2\sin^3\varphi_1\cos\varphi_1 \\ \sin^2\varphi_1\cos^2\varphi_1 & \cos^4\varphi_1 & 0 & 0 & 0 & 2\sin\varphi_1\cos^3\varphi_1 \\ 0 & 0 & 0 & 0 & 0 & 0 \\ 0 & 0 & 0 & 0 & 0 & 0 \\ 0 & 0 & 0 & 0 & 0 & 0 \\ 2\sin^3\varphi_1\cos\varphi_1 & 2\sin\varphi_1\cos^3\varphi_1 & 0 & 0 & 0 & 4\sin^2\varphi_1\cos^2\varphi_1 \end{bmatrix} + N_{V2}\bar{A}_2(\bar{B}_{N2}-\bar{B}_{T2}) \times \begin{bmatrix} \sin^4\varphi_2 & \sin^2\varphi_2\cos^2\varphi_2 & 0 & 0 & 0 & 2\sin^3\varphi_2\cos\varphi_2 \\ 0 & \cos^4\varphi_2 & 0 & 0 & 0 & 2\sin\varphi_2\cos^3\varphi_2 \\ 0 & 0 & 0 & 0 & 0 & 0 \\ 0 & 0 & 0 & 0 & 0 & 0 \\ 0 & 0 & 0 & 0 & 0 & 0 \\ 2\sin^3\varphi_2\cos\varphi_2 & 2\sin\varphi_2\cos^3\varphi_2 & 0 & 0 & 0 & 4\sin^2\varphi_2\cos^2\varphi_2 \end{bmatrix}, \tag{17}$$

where φ_2 is the azimuthal angle to the fracture set with label 2. In each of these special cases, there is a corresponding reduction in the number of degrees of freedom; in what follows we consider the general case, with 8 degrees of freedom (3 elements of α and 5 of β).

If the background medium is isotropic or transversely isotropic and there are at least two non-orthogonal vertical fracture sets, this leads to monoclinic symmetry of the fractured rock, with a stiffness matrix given by:

$$C_{Mono.} = \begin{bmatrix} C_{11} & C_{12} & C_{13} & 0 & 0 & C_{16} \\ C_{12} & C_{22} & C_{23} & 0 & 0 & C_{26} \\ C_{13} & C_{23} & C_{33} & 0 & 0 & C_{36} \\ 0 & 0 & 0 & C_{44} & C_{45} & 0 \\ 0 & 0 & 0 & C_{45} & C_{55} & 0 \\ C_{16} & C_{26} & C_{36} & 0 & 0 & C_{66} \end{bmatrix}, \tag{18}$$

and a compliance matrix of similar form. We can choose axes x_1 and x_2 such that $C_{45}=0$; this is the principal coordinate system. In the present context, where the azimuthal anisotropy is caused by fractures, this choice of coordinate system diagonalizes α_{ij} (Sayers 1998). Therefore, for a vertically propagating shear wave, the fast and slow polarization directions will be in the direction of x_1 and x_2, which coincide with the principal directions of α_{ij}. For a coordinate system not so aligned, the azimuth φ_{S1} of the fast vertical shear wave is given by (Sayers 1998):

$$\tan(2\varphi_{S1}) = 2\alpha_{12}/(\alpha_{11} - \alpha_{22}). \tag{19}$$

This angle may be determined in the field, from the polarization of the fast shear wave measured in a well or a vertical seismic profile.

An important issue in fracture modelling for seismic exploration is the choice of coordinate system. In real world problems, the azimuthal orientation of fractures is usually unknown. Therefore, the problem of characterizing fractured reservoirs should be analysed without assuming that these orientations are known. Taking into account the generality of coordinate systems, the fracture compliance matrix in this work can be categorized into 6 classes by considering the following criteria:

(1) Isotropic or polar anisotropic ('VTI') background
(2) One or more sets of fractures, not necessarily perfectly aligned within any set
(3) Alignment or non-alignment of fractures with the coordinate axes.

The effective compliance tensor S_{ijkl} can be calculated using equation (6). Since seismologists require the stiffness tensor instead, when the fracture compliance ΔS is small, one can directly calculate the stiffness matrix using the additional compliance due to fractures, ΔS_{ijkl} and the background stiffness matrix $\mathbf{C}_0$ (e.g., Sayers 2009):

$$C = C_0 - C_0\,\Delta S\,C_0. \tag{20}$$

We will assume a polar anisotropic background. An isotropic background is a special case of this. In order to maintain generality, each fracture is characterized by its excess compliance, not by its shape or size, which we do not specify here.

The additional compliance, ΔS, due to two or more sets of aligned vertical fractures, not aligned with the coordinate system, has the form:

$$\Delta S = \begin{bmatrix} \alpha_{11}+\beta_{1111} & \beta_{1122} & 0 & 0 & 0 & \alpha_{12}+2\beta_{1112} \\ \beta_{1122} & \alpha_{22}+\beta_{2222} & 0 & 0 & 0 & \alpha_{12}+2\beta_{1222} \\ 0 & 0 & 0 & 0 & 0 & 0 \\ 0 & 0 & 0 & \alpha_{22} & \alpha_{12} & 0 \\ 0 & 0 & 0 & \alpha_{12} & \alpha_{11} & 0 \\ \alpha_{12}+2\beta_{1112} & \alpha_{12}+2\beta_{1222} & 0 & 0 & 0 & \alpha_{11}+\alpha_{22}+4\beta_{1122} \end{bmatrix}, \tag{21}$$

which is the same as equation (8), for this special case.

REFLECTIVITY AND GENERALIZED ANISOTROPY PARAMETERS

In this study, the elastic contrast between the overburden and reservoir will be assumed to be small. In this situation, the plane-wave P-wave reflection coefficient for a plane separating media with arbitrary elastic symmetry with weak anisotropy (WA) can be written in the form (Pšenčík and Martins 2001):

$$\begin{aligned} R_{PP}(\theta,\phi) = {} & R_{PP}^{iso}(\theta) + \frac{1}{2}\Delta\varepsilon_z + \frac{1}{2}\Bigg[\left(\Delta\delta_x - 8\frac{\overline{V_s}^2}{\overline{V_p}^2}\Delta\gamma_x\right)\cos^2\phi \\ & + \left(\Delta\delta_y - 8\frac{\overline{V_s}^2}{\overline{V_p}^2}\Delta\gamma_y\right)\sin^2\phi \\ & + 2\left(\Delta\chi_z - 4\frac{\overline{V_s}^2}{\overline{V_p}^2}\Delta\varepsilon_{45}\right)\cos\phi\sin\phi - \Delta\varepsilon_z\Bigg]\sin^2\theta \\ & + \frac{1}{2}[\Delta\varepsilon_x\cos^4\phi + \Delta\varepsilon_y\sin^4\phi + \Delta\delta_z\cos^2\phi\sin^2\phi \\ & + 2(\Delta\varepsilon_{16}\cos^2\phi + \Delta\varepsilon_{26}\sin^2\phi)\cos\phi\sin\phi] \\ & \times\ \sin^2\theta\tan^2\theta, \end{aligned} \tag{22}$$

where $R_{PP}^{iso}(\theta)$ denotes the weak-contrast reflection coefficient at an interface separating two slightly different isotropic media and the generalized Thomsen anisotropy parameters (Thomsen 1986) are given by Pšenčík and Martins (2001) for each medium:

$$\begin{aligned} & \delta_x = \frac{A_{13}+2A_{55}-V_P^2}{V_P^2}, \quad \delta_y = \frac{A_{23}+2A_{44}-V_P^2}{V_P^2}, \\ & \delta_z = \frac{A_{12}+2A_{66}-V_P^2}{V_P^2}, \quad \chi_z = \frac{A_{36}+2A_{45}}{V_P^2}, \quad \varepsilon_{16} = \frac{A_{16}}{V_P^2}, \\ & \varepsilon_{26} = \frac{A_{26}}{V_P^2}, \quad \varepsilon_{45} = \frac{A_{45}}{V_S^2} \\ & \varepsilon_x = \frac{A_{11}-V_P^2}{2V_P^2}, \quad \varepsilon_y = \frac{A_{22}-V_P^2}{2V_P^2}, \quad \varepsilon_z = \frac{A_{33}-V_P^2}{2V_P^2}, \\ & \gamma_x = \frac{A_{55}-V_S^2}{2V_S^2}, \quad \gamma_y = \frac{A_{44}-V_S^2}{2V_S^2}, \end{aligned} \tag{23}$$

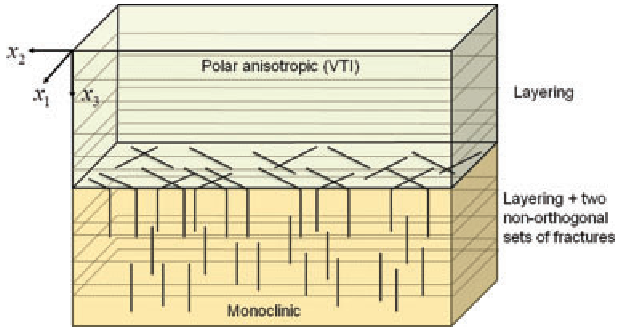

Figure 5 Symmetry types considered for incident medium (polar) and reservoir (monoclinic).

where V_P and V_S are the P- and S-wave velocities of the background isotropic medium, respectively and $A_{\alpha\beta} = C_{\alpha\beta}/\rho$ are the density-normalized elastic stiffness.

The differences (in equation (22)) across the plane in anisotropic parameters are, for example, $\Delta\varepsilon_x = \varepsilon_x^{\text{lower}} - \varepsilon_x^{\text{upper}}$.

For reflectivity modelling in this study, a two layer model will be assumed, where the overburden is assumed to be polar anisotropic and the underlying reservoir is assumed to consist of different sets of fractures embedded in a different polar anisotropic medium, see Fig. 5.

ROTATIONALLY INVARIANT FRACTURES WITH VTI BACKGROUND

If we have an arbitrary number of vertical fractures with rotationally invariant shear compliance, in a polar anisotropic background reservoir, yielding a stiffness matrix C_{ij}, the generalized anisotropy parameters $\delta_x, \delta_y, \delta_z, \chi_z, \varepsilon_x, \varepsilon_y, \varepsilon_z, \varepsilon_{16}, \varepsilon_{26}, \varepsilon_{45}, \gamma_x$and γ_y of the reservoir that were defined before (equations (23)), for an isotropic background, are given in terms of the fracture tensors and VTI background normalized stiffness matrix as:

$$\delta_x = \delta^w + \frac{\Delta C_{13}^f + 2\Delta C_{55}^f}{C_{33}^{VTI}}, \quad \delta_y = \delta^w + \frac{\Delta C_{23}^f + 2\Delta C_{44}^f}{C_{33}^{VTI}},$$
$$\delta_z = 2\varepsilon + \frac{\Delta C_{12}^f + 2\Delta C_{66}^f}{C_{33}^{VTI}}, \quad \chi_z = \frac{\Delta C_{36}^f + 2\Delta C_{45}^f}{C_{33}^{VTI}},$$
$$\varepsilon_{16} = \frac{\Delta C_{16}^f}{C_{33}^{VTI}}, \quad \varepsilon_{26} = \frac{\Delta C_{26}^f}{C_{33}^{VTI}}, \quad \varepsilon_{45} = \frac{\Delta C_{45}^f}{C_{55}^{VTI}}$$
$$\varepsilon_x = \varepsilon + \frac{\Delta C_{11}^f}{2C_{33}^{VTI}}, \quad \varepsilon_y = \varepsilon + \frac{\Delta C_{22}^f}{2C_{33}^{VTI}}, \quad \varepsilon_z = \frac{\Delta C_{33}^f}{2C_{33}^{VTI}},$$
$$\gamma_x = \frac{\Delta C_{55}^f}{2C_{55}^{VTI}}, \quad \gamma_y = \frac{\Delta C_{44}^f}{2C_{55}^{VTI}}, \tag{24}$$

where $\Delta C^f = -C^{VTI}\Delta S C^{VTI}$ is the stiffness matrix due to the fractures, with C_{ij}^{VTI} being the components of the stiffness matrix of the background VTI medium. δ^w is the fully linearized version of Thomsen's δ parameter, valid for weak polar anisotropy:

$$\delta^w \equiv \frac{C_{13}^{VTI} - (C_{33}^{VTI} - 2C_{55}^{VTI})}{C_{33}^{VTI}}, \tag{24a}$$

and ε is the standard VTI parameter defined by Thomsen (1986). The shear-wave VTI parameter γ does not appear in this P-wave problem. In terms of the specific compliance matrices, these parameters are presented in Appendix B.

Substitution of expressions for the anisotropy parameters in terms of α_{ij} and β_{ijkl} into equation (22) allows the sensitivities of the result (to α_{ij} and β_{ijkl}) to be determined, as functions of background parameters and angular aperture. To do this, we recast equation (22) (but with a polar anisotropic background), using sensitivities F_{ij} and F_{ijkl} of $R_{\text{PP}}(\theta,\varphi)$ (defined as the angle-dependent coefficients of the parameters in equation (22)) as follows (Pšenčík and Martins 2001; Sayers 2009):

$$\begin{aligned} R_{PP}(\theta,\phi) = {} & R_{PP}^{iso}(\theta) + R_{PP}^{aniso.}(\theta) + F_{11}(\theta,\phi)\alpha_{11} + F_{12}(\theta,\phi)\alpha_{12} \\ & + F_{22}(\theta,\phi)\alpha_{22} + F_{1111}(\theta,\phi)\beta_{1111} \\ & + F_{1112}(\theta,\phi)\beta_{1112} + F_{1122}(\theta,\phi)\beta_{1122} \\ & + F_{1222}(\theta,\phi)\beta_{1222} + F_{2222}(\theta,\phi)\beta_{2222}. \end{aligned} \tag{25}$$

Equations for sensitivities F_{ij} and F_{ijkl} are given in Appendix C.

INVERSION OF FRACTURE PARAMETERS FROM SYNTHETIC AVOA DATA

In this section we examine the accuracy of inversion for the components of the effective additional compliance matrix (or second- and fourth-rank fracture tensors) from synthetic AVOA data. Synthetic plane-wave PP-reflection data are calculated using known elastic parameters and equation (22). Random noise (S/N = 2) is added. Two fracture azimuths are assumed, at –30° and +50°, with respect to the x_1 direction; this leads to monoclinic symmetry for the fractured medium. The fracture sets have different fracture densities, with 70% of the contribution to the trace of α_{ij} coming from one set and 30% from the other set. Fracture compliances were chosen to give an overall 10% vertical shear-wave splitting if all

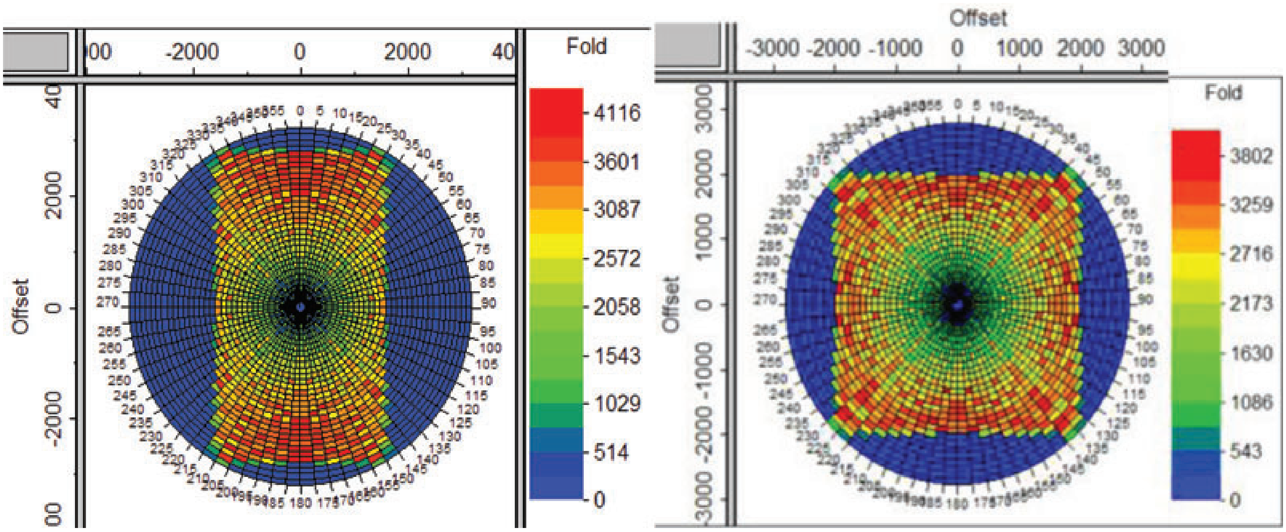

Figure 6 Wide and narrow azimuth data obtained using different acquisition parameters, with the long axis aligned along x_1 (length units are in metres).

fractures were parallel. For the examples considered here (gas shale), two azimuth ranges are considered;

(1) Wide azimuth seismic data with Az = [0,90] and

(2) 'Narrow azimuth' data with Az = [0,45] at the farthest offsets (see Fig. 6).

This choice of azimuths in the modelled NAZ survey obviously affects which particular elements of the specific compliance tensors are well-resolved in the analysis below. The NAZ survey shown in Fig. 6 has an aspect ratio of 0.5 whereas in conventional towed-stream marine acquisition, this ratio may lie between 0.04–0.1, which obviously is not suitable for determining the azimuthal variations discussed herein.

These synthetic data are inverted assuming arbitrary sets of vertical fractures with rotationally invariant shear compliance embedded in a polar anisotropic background; hence we invert only for the fracture compliance matrices α and β. The input to the inversion is the reflectivity (as a function of the angles); it is outside the scope of this work to deduce this reflectivity from the amplitudes of received data, as a function of offset, where deduction involves many issues (e.g., propagation effects and source-configuration effects) not considered here. However, for the inversion, the azimuthally invariant parts of the reflectivity, $R_{PP}^{iso}(\theta)$ and $R_{PP}^{aniso}(\theta)$ are assumed to be imperfectly known and the robustness of the azimuthal inversion to this source of error is investigated below.

Depending on the extent of the fractured area and also the survey design geometry, one can stack the seismic data in different azimuth intervals to give an increase in fold and signal-to-noise ratio (S/N) as required. In this work, the reflectivity data are assumed to be sparse (assumed to be stacked in intervals of 5 degrees). Therefore high-quality reflection data are assumed to be available at 5 degree steps in azimuth and 2 degree steps in offset.

Results of inversion using synthetic reflectivity data with S/N = 2 will be shown; the background media are based upon reservoirs with published data in the literature. For analysing the effect of uncertainty in elastic parameter assumptions and also the effect of background media contrast, data with higher S/N (S/N = 4) will be used, in order to extract meaningful conclusions that are less affected by random noise in reflectivity data. For computing the synthetic reflectivity, fractures were assumed to have rotationally invariant shear compliance and it was assumed that $B_N/B_T = 0.75$, a reasonable value for gas shales (Sayers and Kachanov 1995). This, along with the additional trigonometric factors in β (c.f. equations (11) and (12)), mean that the components of β will be much smaller than those of α (these differences would not be so pronounced for liquid-filled fractures).

Parameters given by Shan *et al.* (2010) for Woodford shale, listed in Table 1, were used for the background media. It is assumed that the upper Woodford, which overlies the reservoir, is not fractured and has VTI symmetry. Vertical elastic parameters for the upper Woodford are listed in Table 1 and its VTI anisotropy parameters are taken to be: $\varepsilon = 0.1$, $\delta = 0.1$ and $\gamma = 0.1$. Shan *et al.* (2010) used these parameters for forward modelling. Note that, since $\varepsilon = \delta$, these values imply

Table 1 Parameters for Woodford shale (Bayuk *et al.* 2009; Shan *et al.* 2010).

Woodford Shale	Depth (km)	Thickness (m)	V_{PO} [krn/s]	V_{SO} [km/s]	V_{P0}/V_{S0}	Density (g/cc)	ε	δ	γ
Upper	~4	9.144	4.509	2.855	1.58	2.855	0.1	0.1	0.1
Middle	~4	53.34	4.161	2.687	1.55	2.46	0.29	0.17	0.1

elliptical P-wave fronts, which is a special case, not necessarily realistic, which leads to difficulties in converting reflection arrival times to depths (Thomsen 1986). However, this does not create any difficulties in this study.

It is also assumed that the middle Woodford is the reservoir and has two sets of vertical and non-orthogonal fractures that lead to monoclinic symmetry (see Fig. 5). Background elastic parameters for the middle Woodford are again selected from Table 1 but anisotropy parameters are chosen from Bayuk *et al.* (2009) who reported anisotropy parameters for 3 samples from the Woodford shale that showed positive anellipticity (i.e., ε-δ > 0). Since their measurements for different samples agree with each other, background VTI anisotropy parameters measured by Bayuk *et al.* (2009) were used for the middle Woodford: $\varepsilon = 0.29$, $\delta = 0.17$ and $\gamma = 0.1$. These VTI parameters are not small, as strictly required by the present theory but this should not affect the present conclusions concerning azimuthal anisotropy, since any errors introduced by the failure of the weak VTI approximation will have azimuthal isotropy. The symmetries of the upper and the middle Woodford are shown in Fig. 5.

The forward problem has the simple form

$$R = Fw, \tag{26}$$

where $\boldsymbol{R}$ is a vector (of length N) containing all data (reflection coefficients), $\boldsymbol{w}$ is a vector (of length M) that represents the unknown parameters (components of the second- and fourth-rank fracture tensors) and $\boldsymbol{F}$ is the $N \times M$ sensitivity matrix. In this problem, $M = 8$. Inversion can be performed using either simple matrix operations, or, more robustly, using the conjugate gradient method that was used in this work. In the first case, the solution can be obtained from

$$w = (F^T F)^{-1} F^T R. \tag{27}$$

Moreover, since for the present AVOA inversion it is assumed that the background (un-fractured) parameters are known, statistical methods for inversion of elastic parameters from post-stack 3D surface seismic data can be used (e.g., Far 2011). Since conventional seismic inversion for isotropic properties will have some error and uncertainty involved, Monte Carlo simulation will be used to take into account the effects of high uncertainty, in the background isotropic and anisotropic parameters, on the inversion results. In order to take into account the uncertainty in the background parameters, 'correct' synthetic reflection data $\boldsymbol{R}$ are computed using constant V_{P0}, V_{S0}, ρ and Thomsen parameters (see Table 1). Then 50 sets of randomly and independently generated V_{P0}, V_{S0}, ρ and Thomsen parameters for the background medium, with standard deviation equal to 15% of the reservoir elastic parameters (see Fig. 7), are used to compute the 'wrong' coefficient matrices contained in $\boldsymbol{F}$ (equation (27) above). Fifty inversions are performed using the 'correct' reflection coefficient data and 50 'wrong' coefficient matrices. In this way, uncertainty is included in the matrix of coefficients or sensitivities. The red line shows the value of the 'correct' parameters used for forward modelling.

Inversion should be preceded by a resolution matrix analysis (Menke 1989) to determine the confidence in the inversion for the fracture tensor components. Resolution matrix analysis is controlled by the seismic data acquisition geometry and the background properties only and should be used to determine an optimum seismic survey design. The resolution matrix is $R_m = \boldsymbol{V}_p \boldsymbol{V}_p^T$ where $\boldsymbol{V}_\mathrm{P}$ is a matrix (not to be confused with the compressional velocity V_P) composed of the significant eigenvalues of $\boldsymbol{F}^T\boldsymbol{F}$ (see Far 2011 for more details). The resolution matrix will be always a square matrix and the magnitudes of its diagonal elements indicate how accurately the inversion determines the corresponding unknown. Figures 8 and 9 show resolution matrices for the WAZ and NAZ data used in this study. The diagonal elements of the matrix represent the resolution of the fracture tensors. Hot colours for diagonal elements imply better resolution than cooler colours.

Singular values are shown at the bottom of figures. The singular values, or s-numbers, are the square roots of the eigenvalues of $\boldsymbol{F}^T\boldsymbol{F}$. The singular values are non-negative real numbers, usually listed in decreasing order ($s_1 > s_2 > s_3 \ldots$). Singular values determine the degree of variation in the matrix of coefficients. In order to obtain a meaningful result from SVD and resolution matrix analysis, insignificant

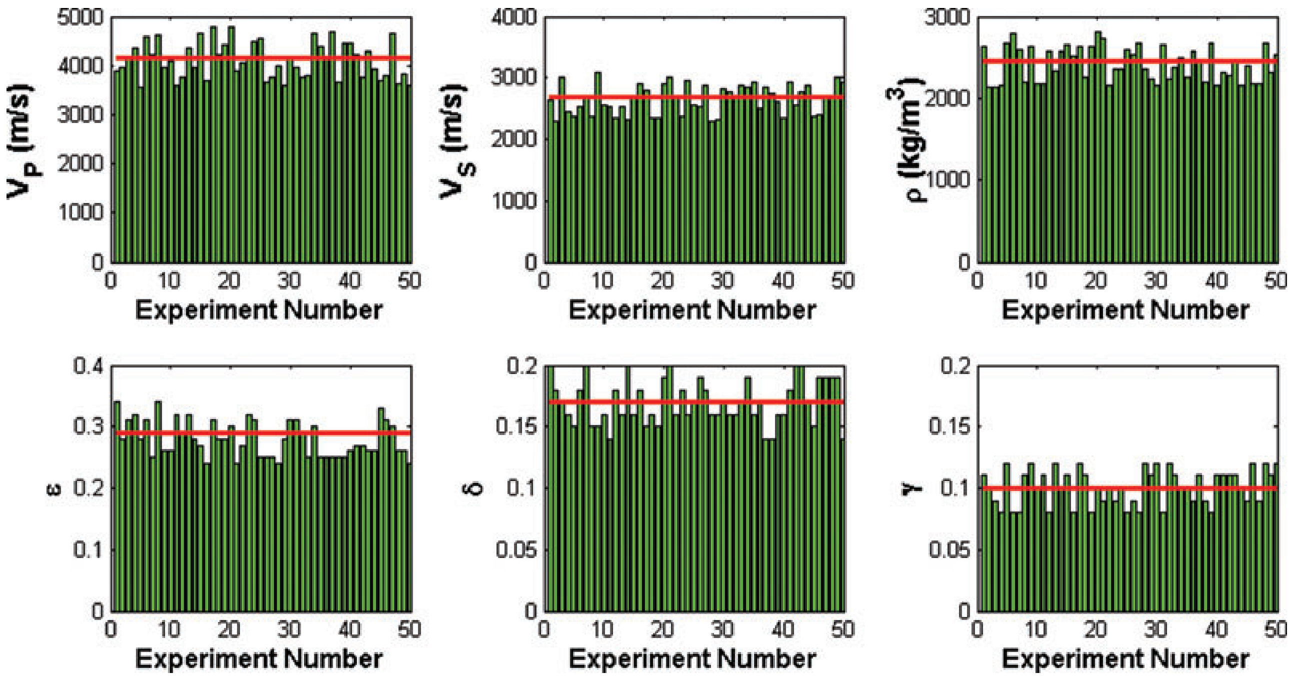

Figure 7 Distributions of randomly generated V_{P0}, V_{S0}, ρ and Thomsen parameters for Monte Carlo simulation. Red line shows the value of parameters used for reflectivity modelling.

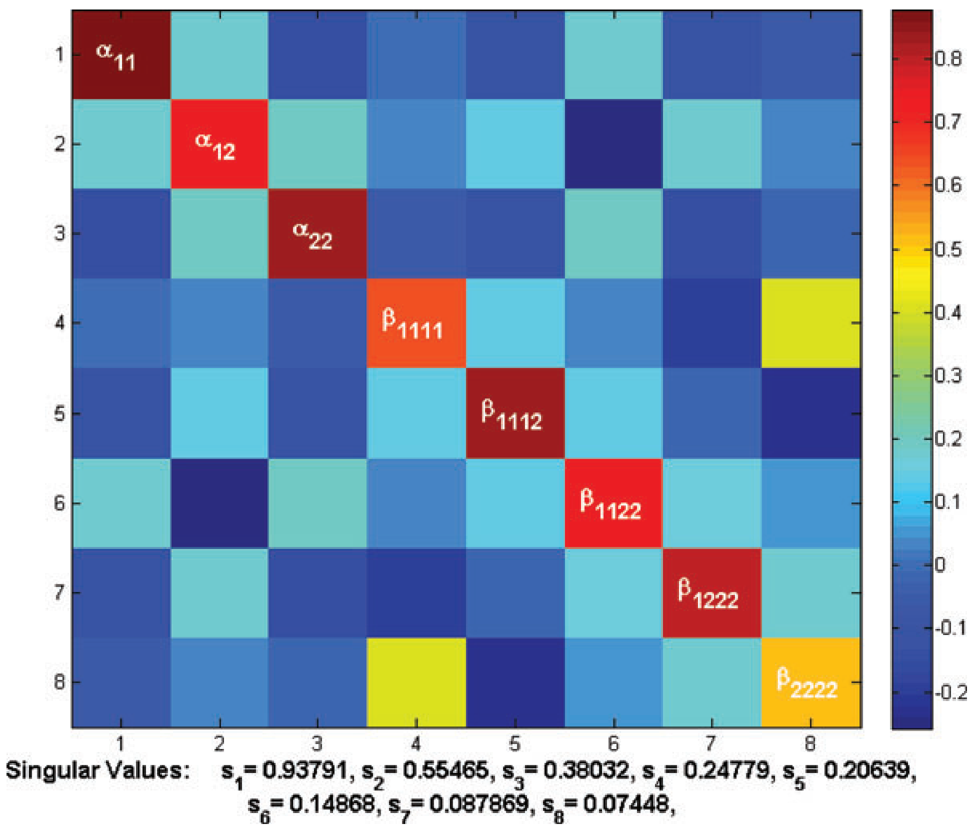

Figure 8 Resolution matrix for wide azimuth seismic data, Woodford shale (fractures with rotationally invariant shear compliance).

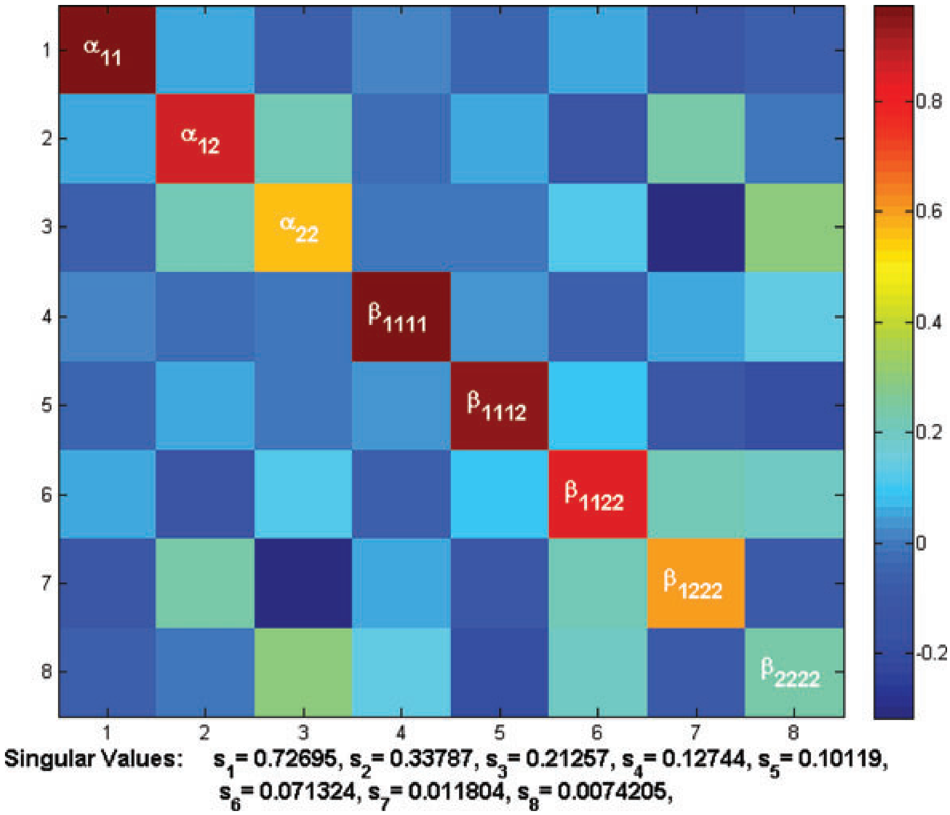

Figure 9 Resolution matrix for narrow azimuth seismic data, Woodford shale (fractures with rotationally invariant shear compliance).

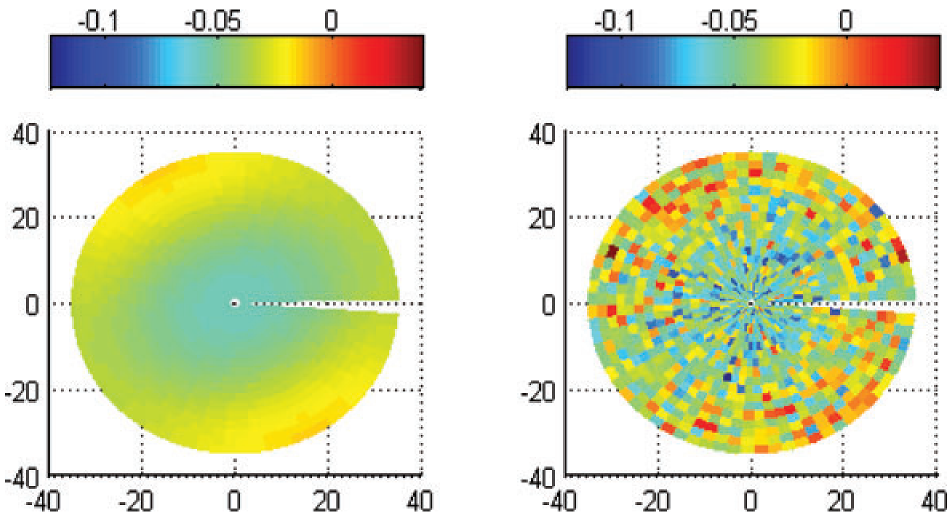

Figure 10 Reflection coefficient plots for the WAZ case showing noise-free reflectivity (left) and noisy reflectivity with $S/N = 2$ (right, used for inversion), with 5 degree stacking intervals.

singular values must be ignored. Determining the right number of insignificant singular values is not always simple. For real world problems, a reliable number can be found by inversion of synthetics and comparing the inversion results to the resolution matrix (as was done in this work). Based on experience from this work, there is no rule of thumb for determining the number of insignificant singular values and this number must be determined by inversion of synthetics and by

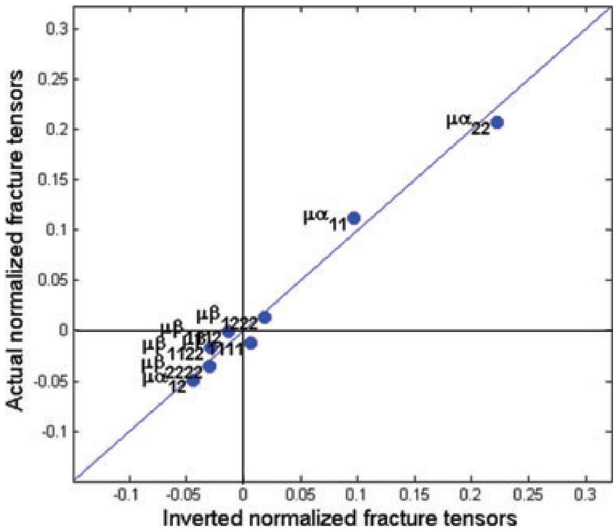

Figure 11 Inversion results of fracture tensors using synthetic reflectivity data with S/N = 2 for the wide azimuth data; correlation coefficient = 98.9%. Vertical axes show the actual normalized fracture tensor values and horizontal axes show the inverted values of the tensors. The components of the second- and fourth-rank fracture tensors are made dimensionless by multiplying by the shear modulus of the background medium ($\mu = \rho {V_{S0}}^2$).

comparing the results of inversion to different resolution matrices (with different numbers of eliminated singular values). For the resolution matrices shown in this study, elimination of 2 singular values showed the best match between the resolution matrix and inversion results.

It should be noted however (as shown in the inversion results) that the results of the resolution matrix will not always be consistent with the inversion results. As mentioned before, SVD is only controlled by the experiment geometry (seismic survey design in this work) and the *a priori* information about the elastic properties of the background unfractured rock. Therefore it is not affected by the quality of the observed data (PP-reflection data in this work) that is used by the inversion.

Inversion with synthetic data has shown that resolution matrices, obtained from data with different geometries, should be interpreted independently (Far 2011). This is because the matrix of sensitivities changes as the geometry changes and as a consequence the eigenvalues (eigenvectors) change. The arrangement of eigenvectors could result in diagonal elements in one resolution matrix that are bigger than in the other resolution matrix. As an example, if in Fig. 9 (NAZ) we have a higher value of β_{1111} than in Fig. 8 (WAZ), it does not mean that β_{1111} will be resolved more successfully using NAZ data rather than using WAZ.

Figure 8 suggests that α_{12}, β_{1111} and β_{2222} will not be resolved accurately with inversion of WAZ PP data. Other components of α and β should be inverted with higher accuracies according to Fig. 8 (compare to Fig. 12). The significance of this resolution matrix is further investigated in the discussion following Figs 7–12.

Figure 9 suggests that α_{22}, β_{1222} and β_{2222} will not be resolved accurately with inversion of this NAZ PP data. Comparison of Figs 8 and 9 suggests that when using these NAZ data, α_{12} will be resolved better than α_{22}, whereas for WAZ data, α_{22} should be resolved better than α_{12}. Another important feature that one can see by comparing the two resolution matrices is that according to Fig. 9, β_{1111} should be one of the well-resolved unknowns but this is not the case for WAZ data, as seen in Fig. 8.

RESULTS

Two inversion cases are considered, based on azimuthal coverage (WAZ or NAZ). Four types of plots are shown for each case: the first plot for each case shows the modelled reflection coefficient. The second plot for each case shows inversion results for fracture tensors using noisy synthetic reflectivity data and knowing the background VTI parameters exactly. The third plot for each case shows the Monte Carlo simulation results; this estimates the inversion errors due to uncertainty in the background parameters. The fourth plot in each case shows the results of Monte Carlo simulation for the predicted direction of the fast vertical shear polarization, as described in Helbig (1994) and Sayers (1998). These fast vertical shear-wave polarization directions are calculated from 50 inversion results of the fracture tensor components shown in the third figures.

Inversion using WAZ seismic data

In this section, results are presented for inversion of α and β using WAZ data for vertical fractures (with rotationally invariant shear compliance). The signal-to-noise ratio of the reflectivity data is 2. Theoretically this WAZ case should be the easiest case for the inversion of fractured medium elastic properties with monoclinic symmetry.

Figure 10 shows the synthetic WAZ reflectivity data. Figure 11 shows that the components of the second-rank fracture tensors α are inverted with high accuracy when we use WAZ data. The errors in the fourth-rank tensor β are about the same size but the components themselves are much smaller, so their relative errors are much bigger.

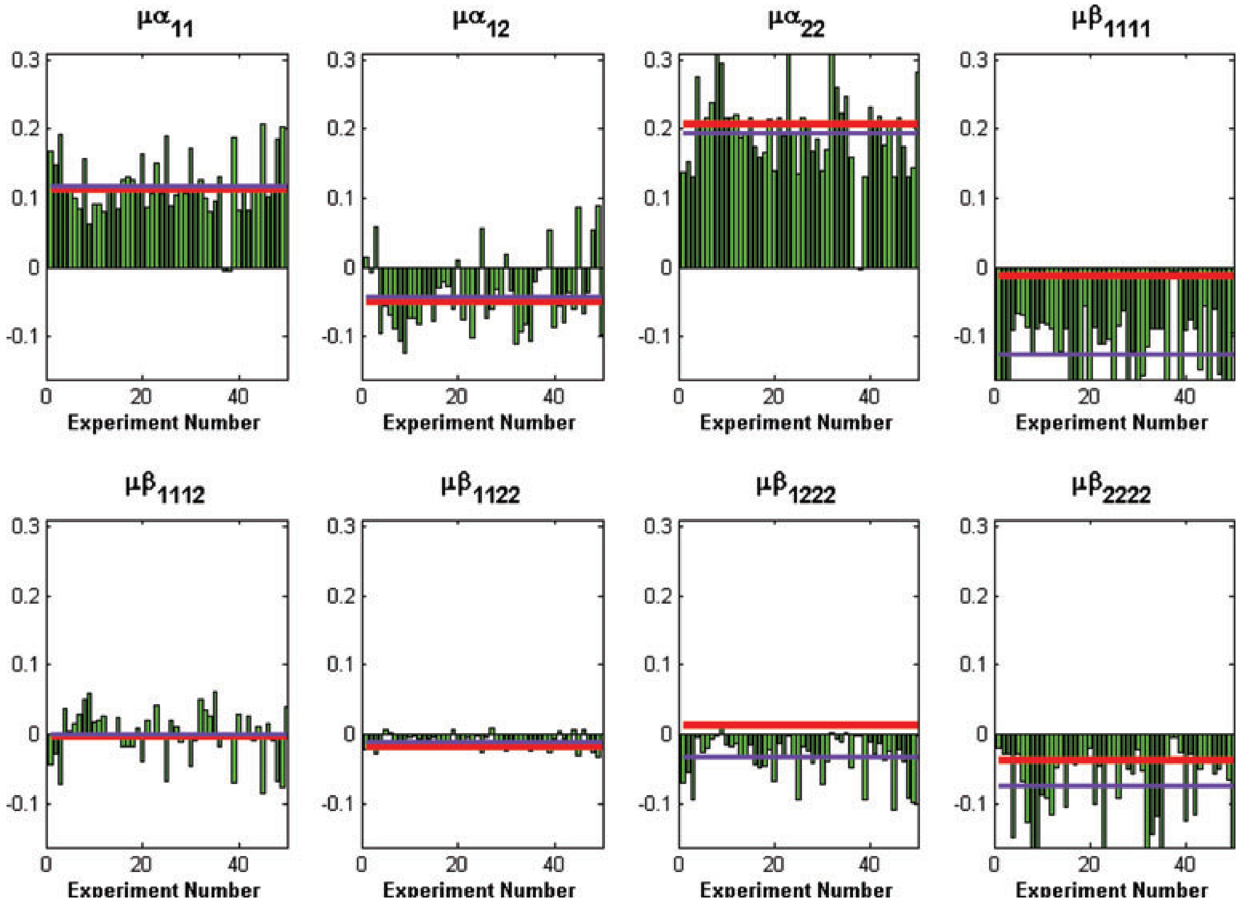

Figure 12 Monte Carlo simulation results using WAZ data with S/N = 2. Red lines show the actual values of the fracture tensor components obtained by forward modelling and purple lines show the average values obtained from 50 inversions. The vertical axes show the values of components of the fracture tensors obtained from inversion and the horizontal axes shows the number of inversions ($\mu = \rho V_{S0}{}^2$).

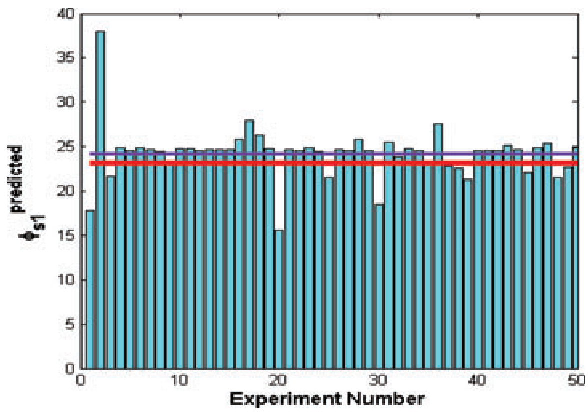

Figure 13 Monte Carlo simulation results for calculation of the fast shear-wave polarization direction from fracture tensor components, WAZ. The vertical axes show the values obtained from the predicted direction of fast shear polarization and the horizontal axes show the number of inversions. Red bars show the actual values of the direction of fast shear polarization and purple bars show the average values obtained from 50 inversions.

Figure 12 shows that α is inverted with a reasonable accuracy. Some components of $\boldsymbol{\beta}$ however (β_{1111}, β_{1222} and β_{2222}) are poorly resolved, as expected according to the resolution matrix shown in Fig. 8, showing the usefulness of the resolution matrix for this case. There is an inconsistency between the corresponding resolution matrix and these results and β_{1111} should have been resolved better than β_{2222}, which is not seen in the inversion results. This suggests careful use of the resolution matrix for real world problems, after observing a consistency in inversion of synthetics.

Figure 13 shows that the direction of the fast shear-wave polarization, which is computed using the second-rank tensor, is inverted with good accuracy as well.

Inversion using NAZ seismic data

Figure 14 shows the synthetic NAZ reflectivity data. In this section, results of inversion for $\boldsymbol{\alpha}$ and $\boldsymbol{\beta}$ using NAZ

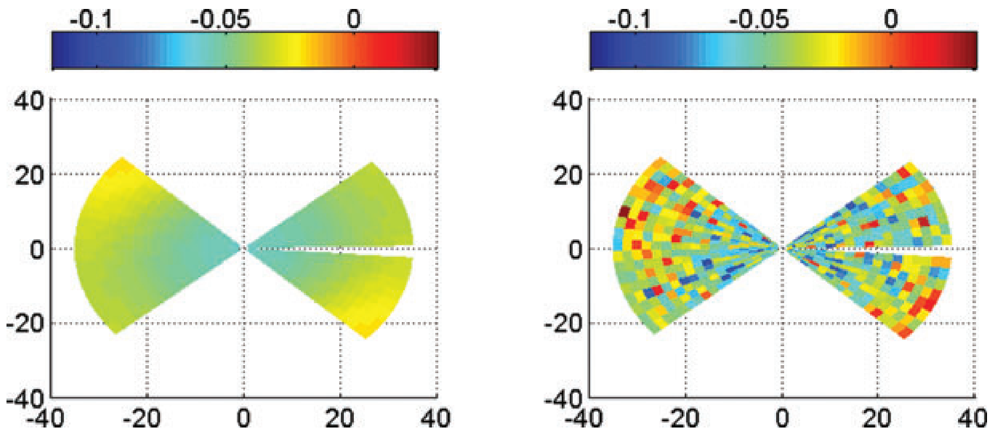

Figure 14 Reflection coefficient plots for the NAZ case showing noise-free reflectivity (left) and noisy reflectivity with S/N = 2 (right, used for inversion), with 5 degree stacking intervals.

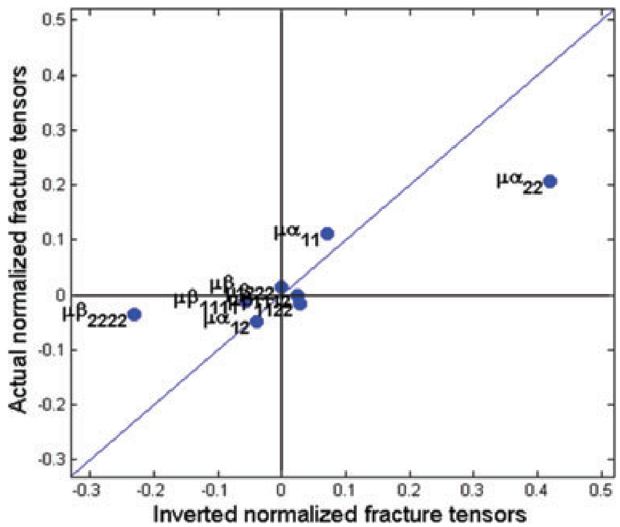

Figure 15 Inversion results of fracture tensors using synthetic reflectivity data with S/N = 2 for narrow azimuth data; correlation coefficient = 88.9%. Vertical axes show the actual normalized fracture tensor values and horizontal axes show the inverted values of the tensors. The components of the second- and fourth-rank fracture tensors are made dimensionless by multiplying by the shear modulus of the background medium ($\mu = \rho {V_{S0}}^2$).

data with the assumption of having arbitrary sets of vertical fractures (with rotationally invariant shear compliance) are presented. The signal-to-noise ratio of the reflectivity data is 2.

Figure 15 shows that, compared to WAZ analysis, NAZ predictions of some components of the second- and fourth-rank fracture tensors (α_{22} and β_{2222}) start to deviate from actual values. However, this degradation in accuracy is less marked for some components than for others, because of the selection of azimuths in this NAZ exercise.

As shown in Fig. 16, the first two components of $\boldsymbol{\alpha}$ are inverted with better accuracy compared to the other components. As predicted by the resolution matrix (Fig. 9), α_{22} cannot be inverted successfully for this NAZ case. It should be noted however that there is not full agreement between the resolution matrix and the inversion results. For example, as seen in Fig. 16, β_{1111} is not resolved accurately and also β_{1222} is poorly resolved compared to β_{2222}.

Since some components of α could not be resolved accurately, the direction of the fast shear- wave polarization could not be inverted successfully (see Fig. 17).

Effect of uncertainty in background elastic properties

In order to further investigate the effect of uncertainty in the VTI parameters, prediction errors of the components of $\boldsymbol{\alpha}$ and $\boldsymbol{\beta}$ were calculated using different degrees of uncertainty. Errors were calculated from the differences between the mean values obtained from 50 realizations of Monte Carlo simulation and the actual values. In order for results and conclusions to be less affected by random noise, higher S/N (S/N = 4) was considered for the analysis. Figure 18 shows error plots in predicting the second- and fourth-rank tensors, using WAZ and NAZ data, as functions of degree of uncertainty in elastic VTI parameters of the background medium (see Fig. 7). The

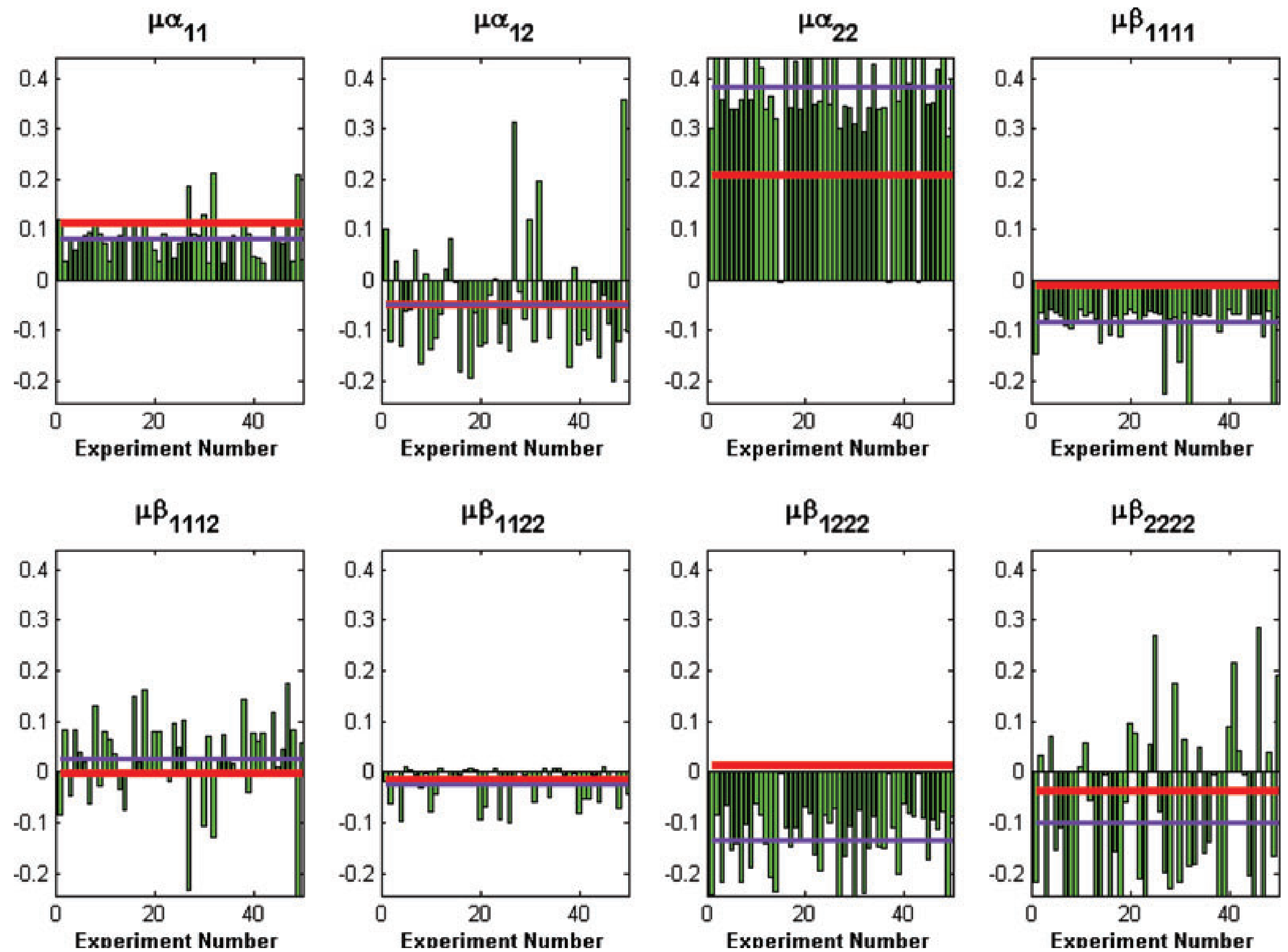

Figure 16 Monte Carlo simulation results using NAZ data with S/N = 2. Red lines show the actual values of the fracture tensor components obtained by forward modelling and purple lines show the average values obtained from 50 inversions ($\mu = \rho V_{S0}{}^2$).

vertical axes show the prediction errors and the horizontal axes show the degrees of uncertainty in the VTI parameters. The actual values of the individual fracture tensor components are shown at the top of each plot. The relative errors are, in general, small for the components of $\boldsymbol{\alpha}$ and large for the components of $\boldsymbol{\beta}$.

DISCUSSION AND CONCLUSION

A method for modelling reservoirs with arbitrary sets of aligned vertical fractures is developed by inversion of synthetic amplitude versus offset and azimuth PP-seismic data, which requires no *a priori* knowledge about the orientation of the fractures. Components of tensors that describe fracture properties, for media with monoclinic or orthotropic symmetry, can be inverted theoretically. Monoclinic and orthotropic symmetries, which take into account layering and lamination of rocks, should be used for anisotropy modelling in fractured rocks.

Based on the inversion results of synthetic WAZ reflection data, inversion of components of the second- and fourth-rank fracture tensors $\boldsymbol{\alpha}$ and $\boldsymbol{\beta}$ (depending on the uncertainties in the *a priori* information about elastic properties of unfractured rock, which was assumed to vary from 0– 30%), have almost the same absolute error. However, the inversion for the components of the fourth-rank fracture tensor $\boldsymbol{\beta}$ has relative errors that are much larger (for this gas-shale case). For NAZ data, the absolute error for α increases (see Figs 11, 15 and 18).

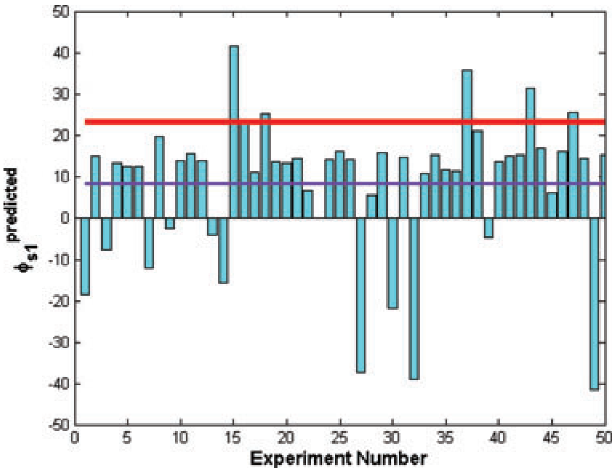

Figure 17 Monte Carlo simulation results for calculation of the fast shear-wave polarization direction from fracture tensor components, NAZ. The vertical axes show the values obtained from the predicted direction of fast shear polarization and the horizontal axes show the number of inversions. Red bars show the actual values of the direction of fast shear polarization and purple bars show the average values obtained from 50 inversions.

In this work, *a priori* knowledge of the number and the direction of fracture sets is not required. Inversion results for the fracture tensors give the most compliant direction in the fractured medium but nothing can be said about the number of fracture sets and the direction of individual fractures, without further assumptions or information. However, if there is *a priori* information about the number of fracture sets, one might be able to predict the fracture orientations. For example if we know that there is only one set of perfectly aligned fractures in the reservoir, in theory their direction can be inverted uniquely. Further conclusions can be reached, using equations (13)–(19), if any of these special cases apply.

Singular value decomposition (SVD) and resolution matrix analysis are controlled by experimental geometry (seismic survey design in this case) and *a priori* information (elastic properties of the unfractured rock in this case). Thus, SVD and/or resolution matrix can be used to determine the optimal seismic survey design for inversion of fracture parameters. Based on inversion results for narrow and wide azimuth survey geometries, high-quality azimuthally varying seismic data

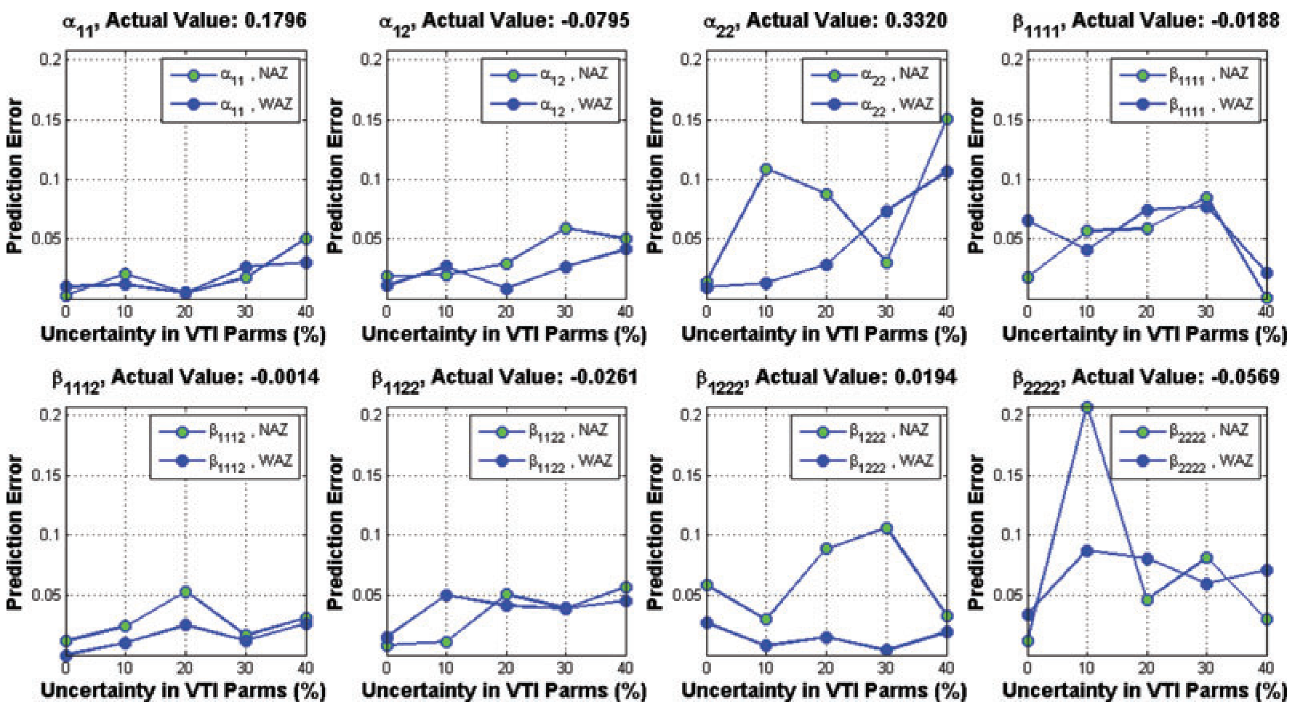

Figure 18 Uncertainty analysis for the WAZ and NAZ cases, with 5 degree stacking intervals and S/N = 4. This figure shows error plots in predicting the second- and fourth-rank tensors, as functions of degree of uncertainty in elastic VTI parameters of the background medium (see Fig. 7). The vertical axes show the prediction errors and the horizontal axes show the degrees of uncertainty in the VTI parameters. The actual values of the individual fracture tensor components are shown on the top of each plot.

with a high-fold number is required to characterize fractures reliably.

REFERENCES

Bayuk I.O., Chesnokov E.M., Ammermann M. and Dyaur N. 2009. Elastic properties of four shales reconstructed from laboratory measurements at unloaded conditions. 79th SEG Annual Meeting, Expanded Abstracts.

Crampin S. 1984. Effective anisotropic constants for wave propagation through cracked solids. *Geophysical Journal of the Royal Astronomical Society* **76**, 135–145.

Eftekharifar M. and Sayers C.M. 2011a. Seismic characterization of fractured reservoirs: A resolution matrix approach. 81st SEG Annual Meeting, Expanded Abstracts.

Eftekharifar M. and Sayers C.M. 2011b. Seismic characterization of fractured reservoirs: Inversion for fracture parameters illustrated using synthetic AVOA data. 81st SEG Annual Meeting, Expanded Abstracts.

Far M.E. 2011. *Seismic Characterization of Naturally Fractured Reservoirs*. PhD dissertation, University of Houston, Houston, TX.

Grechka V. and Kachanov M. 2006. Effective elasticity of rocks with closely spaced and intersecting cracks. *Geophysics* **71**, 85–91.

Helbig K. 1994. *Foundations of Elastic Anisotropy for Exploration Seismic*. Pergamon Press.

Hill R. 1963. Elastic properties of reinforced solids: Some theoretical principles. *Journal of the Mechanics and Physics of Solids* **11**, 357–372.

Jones J.P. and Whittier J.S. 1967. Waves at a flexibly bonded interface. *Journal of Applied Mechanics* **34**, 905–909.

Kachanov M. 1980. Continuum model of medium with cracks. *Journal of the Engineering Mechanics Division of the American Society of Civil Engineers* **106**, no. EMS5, 1039–1051.

Lynn H.B., Bates C.R., Layman M. and Jones M. 1994. Natural fracture characterization using P-wave reflection seismic data, VSP, borehole imaging logs, and in-situ stress field determination. SPE 29595.

Mallick S., Chambers R. E. and Gonzalez A. 1996. Method for determining the principal axes of azimuthal anisotropy from seismic P-wave data. US Patent 5508973.

Menke W. 1989. *Geophysical Data Analysis: Discrete Inverse Theory*. Academic Press.

Nelson R.A. 1985. *Geologic Analysis of Naturally Fractured Reservoirs*. Gulf Publishing Company, Houston.

Nichols D., Muir F. and Schoenberg M. 1989. Elastic properties of rocks with multiple sets of fractures. 59th SEG Annual Meeting, Expanded Abstracts.

Pšenčík I. and Martins J.L. 2001. Properties of weak contrast PP reflection/transmission coefficients for weakly anisotropic elastic media. *Studia Geophysica et Geodaetica* **45**, 176–199.

Reiss L.H. 1980. *The Reservoir Engineering Aspects of Fractured Formations*. Editions Technip, Paris.

Rueger A. 1997. P-wave reflection coefficients for transversely isotropic media with vertical and horizontal axis of symmetry. *Geophysics* **62**, 713–722.

Sayers C.M. 1998. Misalignment of the orientation of fractures and the principal axes for P- and S-waves in rocks containing multiple non-orthogonal fracture sets. *Geophysical Journal International* **133**, 459–466.

Sayers C.M. 2009. Seismic characterization of reservoirs containing multiple fracture sets. *Geophysical Prospecting* **57**, 187–192.

Sayers C.M. and Dean S. 2001. Azimuth-dependent AVO in reservoirs containing non-orthogonal fracture sets. *Geophysical Prospecting* **49**, 100–106.

Sayers C.M. and Kachanov M. 1991. A simple technique for finding effective elastic constants of cracked solids for arbitrary crack orientation statistics. *International Journal of Solids and Structures* **12**, 81–97.

Sayers C.M. and Kachanov M. 1995. Microcrack-induced elastic wave anisotropy of brittle rocks. *Journal of Geophysical Research* **100**, 4149–4156.

Sayers C.M. and Rickett J.E. 1997. Azimuthal variation in AVO response for fractured gas sands. *Geophysical Prospecting* **45**, 165–182.

Schoenberg M. 1980. Elastic wave behavior across linear slip interfaces. *Journal of the Acoustical Society of America* **68**, 1516–1521.

Schoenberg M. and Muir F. 1989. A calculus for finely layered anisotropic media. *Geophysics* **54**, 581–589.

Schoenberg M. and Sayers C.M. 1995. Seismic anisotropy of fractured rock. *Geophysics* **60**, 204–211.

Shan N., Tatham R., Sen M.K., Spikes K. and Ruppel S.C. 2010. Sensitivity of seismic response to variations in the Woodford Shale. 80th SEG Annual Meeting, Expanded Abstracts.

Thomsen L. 1986. Weak elastic anisotropy. *Geophysics* **51**, 1954–1966.

Thomsen L. 1995. Elastic anisotropy due to aligned cracks in porous rock. *Geophysical Prospecting* **43**, 805–829.

Worthington M.H. 2008. Interpreting seismic anisotropy in fractured reservoirs. *First Break* **26**, 57–63.

APPENDIX A

SPECIAL CASES

Consider an isotropic background with one set of fractures aligned with x_1 (x_2 along the symmetry axis); this is the principal coordinate system. Substituting the background compliance tensor (the first term on the right-hand side of equation (6)) and the additional compliance tensor (the second term on the right-hand side of equation (6), cf. equations (11) and (12) with $\cos\varphi = 1$), in 2-index form, one obtains:

$$S = \frac{1}{E}\begin{bmatrix} 1 & -\nu & -\nu & 0 & 0 & 0 \\ -\nu & 1 & -\nu & 0 & 0 & 0 \\ -\nu & -\nu & 1 & 0 & 0 & 0 \\ 0 & 0 & 0 & 2(1+\nu) & 0 & 0 \\ 0 & 0 & 0 & 0 & 2(1+\nu) & 0 \\ 0 & 0 & 0 & 0 & 0 & 2(1+\nu) \end{bmatrix} + \begin{bmatrix} 0 & 0 & 0 & 0 & 0 & 0 \\ 0 & \alpha_{22}+\beta_{2222} & 0 & 0 & 0 & 0 \\ 0 & 0 & 0 & 0 & 0 & 0 \\ 0 & 0 & 0 & \alpha_{22} & 0 & 0 \\ 0 & 0 & 0 & 0 & 0 & 0 \\ 0 & 0 & 0 & 0 & 0 & \alpha_{22} \end{bmatrix}$$

$$= \begin{bmatrix} \frac{1}{E} & -\nu/E & -\nu/E & 0 & 0 & 0 \\ -\nu/E & \frac{1}{E}+\alpha_{22}+\beta_{2222} & -\nu/E & 0 & 0 & 0 \\ -\nu/E & -\nu/E & \frac{1}{E} & 0 & 0 & 0 \\ 0 & 0 & 0 & \alpha_{22}+2(1+\nu)/E & 0 & 0 \\ 0 & 0 & 0 & 0 & 2(1+\nu)/E & 0 \\ 0 & 0 & 0 & 0 & 0 & \alpha_{22}+2(1+\nu)/E \end{bmatrix} \tag{A1}$$

which has HTI symmetry (Schoenberg and Sayers 1995). Similarly, one can show that, if the background medium is polar anisotropic, this one set of fractures results in orthotropic symmetry. Similar methods prove that two orthogonal fracture sets (equations (14) and (15)) in an isotropic or polar anisotropic background medium result in orthotropic symmetry and that two non-orthogonal fracture sets (equations (16) and (17)) in an isotropic or polar anisotropic background medium result in monoclinic symmetry.

APPENDIX B

GENERALIZED ANISOTROPY PARAMETERS

In terms of the specific compliance matrices, anisotropy parameters are defined as (with the superscripts ^{VTI} for the background polar anisotropic medium implicit):

$$\varepsilon_x = \varepsilon + \frac{-C_{11}^2(\alpha_{11}+\beta_{1111}) - C_{12}^2(\alpha_{22}+\beta_{2222}) - 2C_{11}C_{12}\beta_{1122}}{2C_{33}}$$

$$\varepsilon_y = \varepsilon + \frac{-C_{12}^2(\alpha_{11}+\beta_{1111}) - C_{11}^2(\alpha_{22}+\beta_{2222}) - 2C_{11}C_{12}\beta_{1122}}{2C_{33}}$$

$$\varepsilon_z = \frac{-C_{13}^2(\alpha_{11}+\beta_{1111}+\alpha_{22}+\beta_{2222}+2\beta_{1122})}{2C_{33}}$$

$$\varepsilon_{16} = -\frac{C_{66}(2C_{11}\beta_{1112}+2C_{12}\beta_{1222}+\alpha_{12}(C_{11}+C_{12}))}{C_{33}}$$

$$\varepsilon_{26} = -\frac{C_{66}(2C_{12}\beta_{1112}+2C_{11}\beta_{1222}+\alpha_{12}(C_{11}+C_{12}))}{C_{33}}$$

$$\varepsilon_{45} = \frac{-C_{45}^2\alpha_{12}}{C_{55}}$$

$$\delta_x = \delta^w + \frac{-C_{13}(C_{11}(\alpha_{11}+\beta_{1111}) + C_{12}(\alpha_{22}+\beta_{2222}) + \beta_{1122}(C_{11}+C_{12})) - 2C_{55}^2\alpha_{11}}{C_{33}}$$

$$\delta_y = \delta^w + \frac{-C_{13}(C_{12}(\alpha_{11}+\beta_{1111}) + C_{11}(\alpha_{22}+\beta_{2222}) + \beta_{1122}(C_{11}+C_{12})) - 2C_{55}^2\alpha_{22}}{C_{33}}$$

$$\delta_z = 2\varepsilon + \frac{C_{11}C_{12}(\alpha_{11}+\beta_{1111}+\alpha_{22}+\beta_{2222}) - \beta_{1122}(C_{11}+C_{12}) - 2C_{66}^2(\alpha_{11}+\alpha_{22}+4\beta_{1122})}{C_{33}}$$

$$\gamma_x = -\frac{C_{55}\alpha_{11}}{2} \tag{B1}$$

$$\gamma_y = -\frac{C_{55}\alpha_{22}}{2}$$

$$\chi_z = \frac{-2C_{66}C_{13}(\alpha_{12}+\beta_{1112}+\beta_{1222}) - 2C_{55}^2\alpha_{12}}{C_{33}}$$

APPENDIX C

SENSITIVITY EQUATIONS

Sensitivities in equation (25) are obtained as:

$$\begin{aligned}
F_{11}(\theta,\phi) = \frac{1}{\mu}\Bigg[&-\frac{C_{13}^2}{4C_{33}} + \Bigg(\cos^2\phi\left(-\frac{C_{11}C_{13}+2C_{55}^2}{C_{33}}\right.\\
&+\left.\frac{4C_{55}\bar{V}_S^2}{\bar{V}_P^2}\right) - \frac{C_{12}C_{13}\sin^2\phi}{C_{33}}\Bigg)\frac{1}{2}\sin^2\theta\\
&+\Bigg(-\frac{C_{11}^2\cos^4\phi}{2C_{33}} - \frac{(C_{11}C_{12}+2C_{66}^2)\cos^2\phi\sin^2\phi}{C_{33}}\\
&-\frac{C_{12}^2\sin^4\phi}{2C_{33}}\Bigg)\frac{1}{2}\sin^2\theta\tan^2\theta\Bigg]
\end{aligned}$$

$$\begin{aligned}
F_{12}(\theta,\phi) = \frac{1}{\mu}\Bigg[&\left(\frac{4C_{55}\bar{V}_S^2}{\bar{V}_P^2} - \frac{2C_{55}^2+2C_{13}C_{66}}{C_{33}}\right)\sin\phi\cos\phi\,\sin^2\theta\\
&+\left(-\frac{(C_{11}+C_{12})C_{66}}{C_{33}}\right)\cos\phi\sin\phi\sin^2\theta\tan^2\theta\Bigg]
\end{aligned}$$

$$\begin{aligned}
F_{22}(\theta,\phi) = \frac{1}{\mu}\Bigg[&-\frac{C_{13}^2}{4C_{33}} + \frac{1}{2}\Bigg[-\frac{C_{12}C_{13}\cos^2\phi}{C_{33}}\\
&+\left(\frac{4C_{55}\bar{V}_S^2}{\bar{V}_P^2} + \frac{-C_{11}C_{13}-C_{55}^2}{C_{33}}\right)\Bigg]\sin^2\phi\sin^2\theta\\
&+\frac{1}{2}\Bigg(-\frac{(C_{12}\cos^2\phi+C_{11}\sin^2\phi)^2}{2C_{33}}\\
&-\frac{2(C_{66}\cos\phi\sin\phi)^2}{C_{33}}\Bigg)\sin^2\theta\tan^2\theta\Bigg]
\end{aligned} \tag{C1}$$

$$\begin{aligned}
F_{1111}(\theta,\phi) = \frac{1}{\mu}\Bigg[&-\frac{C_{13}^2}{4C_{33}} + \frac{1}{2}\left(-\frac{C_{13}(C_{12}\sin^2\phi + C_{11}\cos^2\phi)}{C_{33}}\right)\\
&\times\sin^2\theta - \frac{1}{2}\left(\frac{1}{2C_{33}}(C_{11}\cos^2\phi + C_{12}\sin^2\phi)^2\right)\\
&\times\sin^2\theta\tan^2\theta\Bigg]
\end{aligned}$$

$$\begin{aligned}
F_{1112}(\theta,\phi) = \frac{1}{\mu}\Bigg[&-\frac{2C_{13}C_{66}\cos\phi\sin\phi}{C_{33}}\sin^2\theta\\
&-\left(\frac{2C_{66}(C_{11}\cos^2\phi + C_{12}\sin^2\phi)}{C_{33}}\right)\\
&\times\cos\phi\sin\phi\sin^2\theta\tan^2\theta\Bigg]
\end{aligned}$$

$$\begin{aligned}
F_{1122}(\theta,\phi) = \frac{1}{\mu}\Bigg[&-\frac{C_{13}^2}{2C_{33}} + \frac{1}{2}\\
&\times\left(\frac{C_{13}(C_{11}+C_{12})(2\cos^2\phi - 1)}{C_{33}}\right)\sin^2\theta\\
&+\frac{1}{2}\left(-\frac{C_{11}C_{12} + (3(C_{11}-C_{12})^2)\cos^2\phi\sin^2\phi}{C_{33}}\right)\\
&\times\sin^2\theta\tan^2\theta\Bigg]
\end{aligned}$$

$$\begin{aligned}
F_{1222}(\theta,\phi) = \frac{1}{\mu}\Bigg[&-\frac{2C_{66}C_{13}}{C_{33}}\sin\phi\cos\phi\sin^2\theta\\
&+\left(-\frac{2C_{66}(C_{11}\sin^2\phi + C_{12}\cos^2\phi)}{C_{33}}\right)\\
&\times\sin\phi\cos\phi\sin^2\theta\tan^2\theta\Bigg]
\end{aligned}$$

$$F_{2222}(\theta,\phi) = \frac{1}{\mu}\left[-\frac{C_{13}^2}{4C_{33}} + \frac{1}{2}\right.$$
$$\times\left(-\frac{C_{13}(C_{11}\sin^2\phi + C_{12}\cos^2\phi)}{C_{33}}\right)\sin^2\theta$$
$$\left.+\frac{1}{2}\left(-\frac{(C_{12}\cos^2\phi + C_{11}\sin^2\phi)^2}{2C_{33}}\right)\sin^2\theta\tan^2\theta\right]$$

where $\bar{V}_P = \frac{V_{P01}+V_{P02}}{2}$, $\bar{V}_S = \frac{V_{S01}+V_{S02}}{2}$ are the average properties of the upper and lower media and $\mu = \rho V_{S0}{}^2$. For the special case of an isotropic background, the sensitivity relations, fully linearized, simplify to:

$$F_{11}(\theta,\phi) = \frac{1}{\mu}\left[-\frac{\lambda^2}{4M} - \frac{1}{2}\left(\cos^2\phi\left(\frac{\lambda^2+2\lambda\mu-2\mu^2}{M}\right)\right.\right.$$
$$\left.+\frac{\lambda^2\sin^2\phi}{M}\right)\sin^2\theta - \frac{1}{2}\left(\frac{1}{2}M\cos^4\phi\right.$$
$$\left.+\frac{(\lambda M+2\mu^2)\sin^2\phi\cos^2\phi}{M} + \frac{\lambda^2\sin^4\phi}{2M}\right)$$
$$\left.\times\sin^2\theta\tan^2\theta\right]$$

$$F_{12}(\theta,\phi) = \frac{1}{\mu}\left[\left(-\frac{2\mu(\lambda-\mu)}{M}\right)\sin\phi\cos\phi\sin^2\theta\right.$$
$$\left.-\frac{2\mu(\lambda+\mu)}{M}\cos\phi\sin\phi\sin^2\theta\tan^2\theta\right]$$

$$F_{22}(\theta,\phi) = \frac{1}{\mu}\left[-\frac{\lambda^2}{4M} + \frac{1}{2}\left(\left(-\frac{\lambda^2+2\lambda\mu-2\mu^2}{M}\right)\sin^2\phi\right.\right.$$
$$\left.+\frac{\lambda^2}{2M}(1-2\cos^2\phi)\right)\sin^2\theta$$
$$+\frac{1}{2}\left(-\frac{\lambda^2\cos^4\phi}{2M} - \frac{(\lambda M+2\mu^2)\sin^2\phi\cos^2\phi}{M}\right.$$
$$\left.\left.-\frac{1}{2}M\sin^4\phi\right)\sin^2\theta\tan^2\theta\right] \tag{C2}$$

$$F_{1111}(\theta,\phi) = \frac{1}{\mu}\left[-\frac{\lambda^2}{4M} + \frac{1}{2}\left(-\frac{\lambda^2\sin^2\phi}{M} - \lambda\cos^2\phi + \frac{\lambda^2}{2M}\right)\right.$$
$$\times\sin^2\theta + \frac{1}{2}\left(-\frac{\lambda^2\sin^4\phi}{2M}\right.$$
$$\left.\left.-\frac{1}{2}M\cos^4\phi - \lambda\sin^2\phi\cos^2\phi\right)\sin^2\theta\tan^2\theta\right]$$

$$F_{1112}(\theta,\phi) = \frac{1}{\mu}\left[-\frac{2\mu\lambda}{M}\cos\phi\sin\phi\sin^2\theta - \left(\frac{2\mu\lambda\sin^2\phi}{M}\right.\right.$$
$$\left.\left.+2\mu\cos^2\phi\right)\cos\phi\sin\phi\times\sin^2\theta\tan^2\theta\right]$$

$$F_{1122}(\theta,\phi) = \frac{1}{\mu}\left[-\frac{\lambda^2}{2M} - \frac{1}{2}\left(\frac{\lambda(\lambda+2\mu)}{M}\right)\sin^2\theta\right.$$
$$+\frac{1}{2}\left(-\frac{(\lambda^2+M^2+4\mu^2)\sin^2\phi\cos^2\phi}{M}\right.$$
$$\left.\left.-\lambda(\sin^4\phi+\cos^4\phi)\right)\sin^2\theta\tan^2\theta\right]$$

$$F_{1222}(\theta,\phi) = \frac{1}{\mu}\left[-\frac{2\lambda\mu}{M}\sin\phi\cos\phi\sin^2\theta - \left(\frac{2\lambda\mu\cos^2\phi}{M}\right.\right.$$
$$\left.\left.+2\mu\sin^2\phi\right)\sin\phi\cos\phi\times\sin^2\theta\tan^2\theta\right]$$

$$F_{2222}(\theta,\phi) = \frac{1}{\mu}\left[-\frac{\lambda^2}{4M} + \frac{1}{2}\left(-\lambda\sin^2\phi + \frac{\lambda^2}{2M}(1-2\cos^2\phi)\right)\right.$$
$$\times\sin^2\theta + \frac{1}{2}\left(-\frac{\lambda^2\cos^4\phi}{2M} - \frac{1}{2}M\sin^4\phi\right.$$
$$\left.\left.-\lambda\sin^2\phi\cos^2\phi\right)\sin^2\theta\tan^2\theta\right]$$

where $M = K + 4\mu/3 = \lambda + 2\mu$ is the longitudinal modulus of the reservoir rock in the absence of fractures and K, μ and λ are its bulk modulus, shear modulus and Lame parameter, respectively. In fact, if the sensitivity factors F (of equation (C1)) are fully linearized in the small VTI parameters of the background medium, the result is equation (C2).